Inorg. Chem. **2002**, *41*, 259–277

The OsO_3F^+ and μ-$F(OsO_3F)_2^+$ Cations: Their Syntheses and Study by Raman and ^{19}F NMR Spectroscopy and Electron Structure Calculations and X-ray Crystal Structures of $[OsO_3F][PnF_6]$ (Pn = As, Sb), $[OsO_3F][HF]_2[AsF_6]$, $[OsO_3F][HF][SbF_6]$, and $[OsO_3F][Sb_3F_{16}]$†

Michael Gerken,‡ David A. Dixon,§ and Gary J. Schrobilgen*,‡

Department of Chemistry, McMaster University, Hamilton, Ontario L8S 4M1, Canada, and William R. Wiley Environmental Molecular Sciences Laboratory, Pacific Northwest National Laboratory, 906 Battelle Blvd., P.O. Box 999, KI-83, Richland, Washington 99352

Received July 20, 2001

The fluoride ion donor properties of OsO_3F_2 have been investigated. The salts $[OsO_3F][AsF_6]$, $[OsO_3F][HF]_2[AsF_6]$, μ-$F(OsO_3F)_2[AsF_6]$, $[OsO_3F][HF]_2[SbF_6]$, and $[OsO_3F][HF][SbF_6]$ have been prepared by reaction of OsO_3F_2 with AsF_5 and SbF_5 in HF solvent and have been characterized in the solid state by Raman spectroscopy. The single-crystal X-ray diffraction studies of $[OsO_3F][AsF_6]$ ($P2_1/n$, $a = 7.0001(11)$ Å, $b = 11.0620(11)$ Å, $c = 8.8629(13)$ Å, $\beta = 92.270(7)°$, $Z = 4$, and $R_1 = 0.0401$ at –126 °C), $[OsO_3F][SbF_6]$ ($P2_1/c$, $a = 5.4772(14)$ Å, $b = 10.115(3)$ Å, $c = 12.234(3)$ Å, $\beta = 99.321(5)°$, $Z = 4$, and $R_1 = 0.0325$ at –173 °C), $[OsO_3F][HF]_2[AsF_6]$ ($P2_1/n$, $a = 5.1491(9)$ Å, $b = 8.129(2)$ Å, $c = 19.636(7)$ Å, $\beta = 95.099(7)°$, $Z = 4$, and $R_1 = 0.0348$ at –117 °C), and $[OsO_3F][HF][SbF_6]$ (Pc, $a = 5.244(4)$ Å, $b = 9.646(6)$ Å, $c = 15.269(10)$ Å, $\beta = 97.154(13)°$, $Z = 4$, and $R_1 = 0.0558$ at –133 °C) have shown that the OsO_3F^+ cations exhibit strong contacts to the anions and HF solvent molecules giving rise to cyclic, dimeric structures in which the osmium atoms have coordination numbers of 6. The reaction of OsO_3F_2 with neat SbF_5 yielded $[OsO_3F][Sb_3F_{16}]$, which has been characterized by ^{19}F NMR spectroscopy in SbF_5 and SO_2ClF solvents and by Raman spectroscopy and single-crystal X-ray diffraction in the solid state ($P4\bar{2}_1m$, $a = 10.076(6)$ Å, $c = 7.585(8)$ Å, $Z = 2$, and $R_1 = 0.0858$ at –113 °C). The weak fluoride ion basicity of the $Sb_3F_{16}^-$ anion resulted in an OsO_3F^+ cation (C_{3v} point symmetry) that is well isolated from the anion and in which the osmium is four-coordinate. The geometrical parameters and vibrational frequencies of OsO_3F^+, ReO_3F, μ-$F(OsO_3F)_2^+$, $(FO_3Os\text{--}FPnF_5)_2$, and $(FO_3Os\text{--}(HF)_2\text{--}FPnF_5)_2$ (Pn = As, Sb) have been calculated using density functional theory methods.

Introduction

The fluoride ion donor chemistry of Os(VIII) has thus far been limited to cations derived from *cis*-OsO_2F_4.[1] The latter are formed by reaction of *cis*-OsO_2F_4 with the strong Lewis acid fluoride ion acceptors, AsF_5 and SbF_5. The dinuclear fluorine-bridged $[F_3O_2Os\text{--}F\text{--}OsO_2F_3]^+$ cation exhibits a distorted octahedral *cis*-dioxo arrangement about the osmium atoms in the crystal structure of $[\mu$-$F(OsO_2F_3)_2][Sb_2F_{11}]$, which was isolated by crystallization from SbF_5/HF mixtures. Failure to obtain a crystal structure containing the trigonal bipyramidal $OsO_2F_3^+$ cation is indicative of the reluctance of this osmium(VIII) dioxo species to lower its coordination number below 6. Consequently, the $OsO_2F_3^+$ cation has only been observed by ^{19}F NMR spectroscopy with the weakly nucleophilic, polymeric $Sb_nF_{5n+1}^-$ anion as the counteranion in the highly acidic, strong fluoride ion acceptor solvent, SbF_5.

The fluoride ion acceptor properties of OsO_3F_2 have been established by the formation of the distorted octahedral *fac*-$OsO_3F_3^-$ anion in the salts $[K][OsO_3F_3]$,[2,3] $[Rb][OsO_3F_3]$,[2] $[Cs][OsO_3F_3]$,[2,3] $[Ag][OsO_3F_3]$,[2,3] $[NO][OsO_3F_3]$,[4] and

† Dedicated to our colleague Professor Karl O. Christe on the occasion of his 65th birthday and in appreciation of his long friendship and his many outstanding synthetic and structural contributions to the field of inorganic fluorine chemistry.

* To whom correspondence should be addressed. E-mail: SCHROBIL@McMASTER.CA.

‡ McMaster University.

§ Pacific Northwest National Laboratory.

(1) Casteel, W. J., Jr.; Dixon, D. A.; Mercier, H. P.; Schrobilgen, G. J. *Inorg. Chem.* **1996**, *37*, 340.

10.1021/ic0107680 CCC: $22.00
Published on Web 12/21/2001

$[N(CH_3)_4][OsO_3F_3]$.[4] The preferred coordination number of osmium(VIII) trioxo species also appears to be 6, which has been found for the *fac*-$OsO_3F_3^-$ anion in $[N(CH_3)_4][OsO_3F_3]$[4] as well as in the low-temperature phase of the neutral parent compound, $(OsO_3F_2)_\infty$,[5] which exists as a fluorine bridged polymeric chain in the solid state.

The fluoride ion donor properties of OsO_3F_2 have been investigated for the first time in the present study. Because ReO_3F has been prepared[6] and characterized by vibrational,[7−9] microwave,[10] and UV spectroscopy,[9] the isoelectronic OsO_3F^+ cation was anticipated to be isolable as salts derived from the strong fluoride ion acceptors, AsF_5 and SbF_5.

Results and Discussion

Syntheses of the OsO_3F^+ and $Os_2O_6F_3^+$ Cations and Solution Characterization of the OsO_3F^+ Cation by ^{19}F NMR Spectroscopy. Osmium trioxide difluoride, which is insoluble in HF, reacts with excess AsF_5 in HF according to eq 1, yielding a yellow-orange solution of solvated $[OsO_3F][AsF_6]$. The $[OsO_3F][AsF_6]$ salt is expected to be strongly solvated in HF solvent as suggested by the crystal structure of $[OsO_3F][HF]_2[AsF_6]$ (see X-ray Crystallography, part c). Stoichiometric amounts of AsF_5 did not result in complete dissolution of OsO_3F_2, presumably because of the competing reaction with HF solvent (eq 2) or the need to use the stronger

$$OsO_3F_2 + PnF_5 \xrightarrow{HF,\ RT} [OsO_3F][PnF_6]_{HF} \quad Pn = As, Sb \quad (1)$$

$$2HF + AsF_5 \rightarrow [H_2F][AsF_6] \quad (2)$$

Lewis acid $(AsF_5)_n$ to depolymerize $(OsO_3F_2)_\infty$. Slow removal of the HF solvent at −78 °C initially yielded orange crystals having the composition $[OsO_3F][HF]_2[AsF_6]$ (see X-ray Crystallography, part c). Further pumping at −78 °C resulted in the loss of both HF solvent molecules, yielding straw-yellow $[OsO_3F][AsF_6]$, which was unstable at ambient temperatures, dissociating to OsO_3F_2 and AsF_5. Crystals of solvent-free $[OsO_3F][AsF_6]$ were grown from HF solvent at −78 °C in the presence of an excess of AsF_5 (see X-ray Crystallography, part a).

Attempts to redissolve $[OsO_3F][AsF_6]$ in HF solvent resulted in loss of AsF_5 and precipitation of orange $[Os_2O_6F_3][AsF_6]$ according to eq 3, which was identified by Raman spectroscopy. Removal of HF solvent yielded a mixture of solid $[OsO_3F][AsF_6]$, OsO_3F_2 and small amounts of $[Os_2O_6F_3][AsF_6]$, which were identified by Raman spectroscopy and resulted from partial dissociation according to eq 4. The instability of $[\mu\text{-}F(OsO_3F)_2][AsF_6]$ in the absence of HF solvent suggests stabilization by coordination of HF molecules to the $Os_2O_6F_3^+$ cation. The formation of the $Os_2O_6F_3^+$ cation from $[OsO_3F][AsF_6]$ (eq 3) can be reversed by addition

$$2[OsO_3F][AsF_6] \overset{HF}{\rightleftharpoons} [\mu\text{-}F(OsO_3F)_2][AsF_6] + AsF_5 \quad (3)$$

$$[\mu\text{-}F(OsO_3F)_2][AsF_6] \xrightarrow{-HF,\ RT} [OsO_3F][AsF_6] + OsO_3F_2 \quad (4)$$

of excess AsF_5 to the HF solution. The very low solubility of $[\mu\text{-}F(OsO_3F)_2][AsF_6]$ in HF solvent prevented crystal growth. Solutions of solvated $[OsO_3F][AsF_6]$ in HF solvent are unstable, dissociating to OsO_3F_2 and AsF_5 in under 1 min at room temperature. The ^{19}F NMR spectrum of OsO_3F_2 in the presence of a 13.5-fold molar excess of AsF_5 in HF solvent at −80 °C showed a broad singlet at −132.2 ppm ($\Delta\nu_{1/2}$ = 500 Hz), which is attributed to fast fluorine exchange among the OsO_3F^+ cation, AsF_6^-, $As_2F_{11}^-$, AsF_5, and HF solvent.

At room temperature, OsO_3F_2 was very soluble in HF solutions containing stoichiometric amounts of SbF_5 and yielded a yellow solution of solvated $[OsO_3F][SbF_6]$ (eq 1) from which yellow $[OsO_3F][HF][SbF_6]$ slowly crystallized at −78 °C (see X-ray Crystallography, part d). Removal of HF solvent under vacuum at −78 °C yielded $[OsO_3F][HF][SbF_6]$, which melted at approximately 45 °C and was stable to brief pumping at room temperature but resulted in partial removal of solvated HF upon pumping for more than 5 min at room temperature. Complete conversion to $[OsO_3F][SbF_6]$ was not possible, presumably because the dissociation pressure of coordinated HF is very low at room temperature and competes with the decomposition of $[OsO_3F][SbF_6]$ at temperatures close to and above room temperature. Pumping at 45 °C led to a decrease in the relative Raman intensities of the symmetric Os−O stretching bands assigned to $[OsO_3F][SbF_6]$ when compared with those of $[OsO_3F][HF][SbF_6]$. Although $[OsO_3F][SbF_6]$ could not be isolated in bulk as a pure solid, a crystal of $[OsO_3F][SbF_6]$ suitable for X-ray structure determination was selected from a mixture that had been obtained from an HF solution of $[OsO_3F][SbF_6]$ (see X-ray Crystallography, part b). Upon slow removal of HF solvent from a solution containing solvated $[OsO_3F][SbF_6]$, orange $[OsO_3F][HF]_2[SbF_6]$ crystallized at high concentration. One HF molecule was readily lost under dynamic vacuum at −78 °C, yielding $[OsO_3F][HF][SbF_6]$.

Dissolution of OsO_3F_2 in neat SbF_5 at 55 °C gave rise to a yellow solution according to eq 5. Below 55 °C, the

$$OsO_3F_2 + nSbF_5 \xrightarrow{SbF_5,\ 55\ °C} [OsO_3F][Sb_nF_{5n+1}] \quad (5)$$

solubility of $[OsO_3F][Sb_nF_{5n+1}]$ decreased dramatically and straw-yellow $[OsO_3F][Sb_3F_{16}]$ crystallized from SbF_5 solvent. The empirical formula was established by mass balance after removal of excess SbF_5 at room temperature and was confirmed by X-ray crystallography (see X-ray Crystallography, part e). The weakly fluoro-basic $Sb_3F_{16}^-$ anion is required to stabilize the unsolvated, distorted tetrahedra OsO_3F^+ cation and is indicative of the weak fluoride ion

(2) Jones, P. J.; Levason, W.; Tajik, M. *J. Fluorine Chem.* **1984**, *25*, 195.
(3) Hepworth, M. A.; Robinson, P. L. *Inorg. Nucl. Chem.* **1957**, *4*, 24.
(4) Gerken, M.; Dixon, D. A.; Schrobilgen, G. J. *Inorg. Chem.* **2000**, *39*, 4244.
(5) Bougon, R.; Buu, B.; Seppelt, K. *Chem. Ber.* **1993**, *126*, 1331.
(6) Aynsley, E. E.; Hair, M. L. *J. Chem. Phys.* **1958**, 3747.
(7) Selig, H.; El-Gad, U. *J. Inorg. Nucl. Chem.* **1973**, *35*, 3517.
(8) Beattie, I. R.; Crocombe, R. A.; Ogden, J. S. *J. Chem. Soc., Dalton Trans.* **1977**, 1481.
(9) Brisdon, A. K.; Holloway, J. H.; Hope, E. G.; Townson, P. J.; Levason, W.; Ogden, J. S. *J Chem. Soc., Dalton Trans.* **1991**, 3127.
(10) Lotspeich, J. F.; Javan, A.; Engelbrecht, A. *J. Chem. Phys.* **1959**, *31*, 633.

Table 1. Summary of Crystal Data and Refinement Results for $[OsO_3F][AsF_6]$, $[OsO_3F][SbF_6]$, $[OsO_3F][HF]_2[AsF_6]$, $[OsO_3F][HF][SbF_6]$, and $[OsO_3F][Sb_3F_{16}]$

	$[OsO_3F][AsF_6]$	$[OsO_3F][SbF_6]$	$[OsO_3F][HF]_2[AsF_6]$	$[OsO_3F][HF][SbF_6]$	$[OsO_3F][Sb_3F_{16}]$
formula	AsF_7O_3Os	F_7O_3OsSb	$H_2AsF_9O_3Os$	HF_8O_3OsSb	$F_{17}O_3OsSb_3$
space group	$P2_1/n$ (No. 14)	$P2_1/c$ (No. 14)	$P2_1/n$ (No. 14)	Pc (No. 7)	$P\bar{4}2_1m$ (No. 113)
a (Å)	7.0001(11)	5.4772(14)	5.1491(9)	5.244(4)	10.076(6)
b (Å)	11.0620(11)	10.115(3)	8.129(2)	9.646(6)	10.076(6)
c (Å)	8.8629(13)	12.234(3)	19.636(7)	15.269(10)	7.585(8)
α (deg)	90	90	90	90	90
β (deg)	92.270(7)	99.321(5)	95.099(7)	97.154(13)	90
γ (deg)	90	90	90	90	90
V (Å^3)	685.8(2)	668.8(3)	818.7(4)	766.4(10)	770.1(10)
Z (molecules/unit cell)	4	4	4	4	2
mol wt	446.12	492.95	486.14	512.96	926.45
calcd density (g cm^{-3})	4.321	4.896	3.944	4.446	3.995
μ (mm^{-1})	23.494	23.132	19.730	20.215	13.617
final agreement factors	$R_1{}^a = 0.0401$	$R_1{}^a = 0.0325$	$R_1{}^a = 0.0348$	$R_1{}^a = 0.0558$	$R_1{}^a = 0.0858$
	$wR_2{}^b = 0.0797$	$wR_2{}^b = 0.0772$	$wR_2{}^b = 0.0864$	$wR_2{}^b = 0.1198$	$wR_2{}^b = 0.1871$

^{a} $R_1 = \sum|F_o| - |F_c|/\sum|F_o|$. ^{b} $wR_2 = \sum|(|F_o| - |F_c|)w^{1/2}|/\sum(|F_o|w)$.

donor properties of OsO_3F_2 and the high electrophilicity of the OsO_3F^+ cation. Dissolution of $[OsO_3F][Sb_3F_{16}]$ in HF solvent resulted in a precipitate at −78 °C, which was identified as $[OsO_3F][HF][SbF_6]$ by Raman spectroscopy. Although $[OsO_3F][AsF_6]$ was isolated from HF solutions in the presence of excess AsF_5, unsolvated $[OsO_3F][SbF_6]$ did not form from an HF solution containing a 2-fold molar excess of SbF_5. This may be a consequence of the lower nucleophilicity of SbF_6^- when compared with that of AsF_6^-; therefore, the OsO_3F^+ cation is coordinatively less saturated in the unsolvated SbF_6^- salt so that the vacant osmium coordination site accommodates an HF solvent molecule instead. This reasoning is not, however, corroborated by X-ray crystallographic data, which show stronger Os--F contacts in $[OsO_3F][SbF_6]$ than in $[OsO_3F][AsF_6]$ (see X-ray Crystallography, parts a and b).

The ^{19}F NMR spectrum of OsO_3F_2 dissolved in neat SbF_5 at 55 °C gives rise to a broad singlet for the OsO_3F^+ cation at 70.9 ppm ($\Delta\nu_{1/2} = 360$ Hz) and to broad $Sb_nF_{5n+1}^-/(SbF_5)_n$ resonances at −91.5 (shoulder), −105.7 ppm ($\Delta\nu_{1/2} \approx 5400$ Hz), and −128.1 ($\Delta\nu_{1/2} \approx 5800$ Hz). The ^{19}F resonance of the OsO_3F^+ cation is significantly more shielded than those of the $OsO_2F_3^+$ cation (122.4 and 129.5 ppm),[1] which is consistent with a decrease in the number of strongly electron withdrawing fluorine ligands. This trend, however, is opposite to that observed for xenon(VI) oxide fluorides.[11] The ^{19}F NMR spectrum of $[OsO_3F][Sb_3F_{16}]$ dissolved in SO_2ClF solvent at −100 °C showed a singlet at 77.1 ppm corresponding to the OsO_3F^+ cation. The resonances of the *cis*-fluorine-bridged $Sb_3F_{16}^-$ and $Sb_2F_{11}^-$ anions and of $SO_2ClF{\cdot}SbF_5$ were observed in the F-on-Sb region.[12] The NMR parameters of the anions and the SO_2ClF adduct are in good agreement with the previously reported values.[13,14] Approximately 70% of the $Sb_3F_{16}^-$ anions were dissociated in SO_2ClF solution according to eq 6. In view of the small

$$Sb_3F_{16}^- + SO_2ClF \xrightarrow{SO_2ClF,\ -100\ °C} Sb_2F_{11}^- + SO_2ClF{\cdot}SbF_5 \quad (6)$$

magnitudes of the one-bond $^{187}Os-^{19}F$ coupling constants found for *cis*-OsO_2F_4 (35.1 and 59.4 Hz)[15] and *fac*-$OsO_3F_3^-$ (32 Hz)[4] and the low abundance of ^{187}Os (1.64%), the ^{187}Os satellites are presumably hidden as a consequence of the breath of the central ^{19}F signal ($\Delta\nu_{1/2} = 140$ Hz).

X-ray Crystallography. Details of the data collection parameters and other crystallographic information for $[OsO_3F][AsF_6]$, $[OsO_3F][SbF_6]$, $[OsO_3F][HF]_2[AsF_6]$, $[OsO_3F][HF][SbF_6]$, and $[OsO_3F][Sb_3F_{16}]$ are provided in Table 1, and important bond lengths, angles and contacts are listed in Tables 2 and 3.

(a) $[OsO_3F][AsF_6]$. The crystal structure of $[OsO_3F][AsF_6]$ consists of OsO_3F^+ cations and AsF_6^- anions which are bridged through a fluorine of the AsF_6^- anion. Two cation−anion pairs are linked to each other by two additional Os--F−As bridges forming a cyclic dimer which is located on a crystallographic inversion center (Figure 1). The dimers are, in turn, stacked in columns parallel to the *a* axis (Figure 9, Supporting Information).

The OsO_3F^+ cation is distorted from the expected C_{3v} point symmetry with one Os−O bond that is significantly longer (1.711(8) Å) than the other two (1.674(9) and 1.679(9) Å). Each cation forms two short (2.450(7) and 2.666(7) Å) Os--F contacts and one long (3.072(8) Å) Os···F contact with the fluorines of the AsF_6^- anions. The fluorine contacts are directed through the three less repulsive, trigonal OOF faces of the OsO_3F^+ distorted tetrahedron, and not through the

(11) Gerken, M.; Schrobilgen, G. J. *Coord. Chem. Rev.* **2000**, *197*, 335.

(12) The ^{19}F NMR spectrum of $[OsO_3F][Sb_3F_{16}]$ in SO_2ClF solvent contained signals that are assigned to the $SO_2ClF{\cdot}SbF_5$ adduct (F-on-S, 94.40 ppm (s); F_1, −143.08 ppm (q); F_2, −105.63 ppm (d); $^2J(F_1-F_2) = 96$ Hz), the $Sb_2F_{11}^-$ anion (F_1, −136.04 ppm (q); F_2, −113.79 ppm (dd); F_3, −90.99 ppm (m); $^2J(F_1-F_2) = 103$ Hz; $^2J(F_1-F_3) = 61$ Hz), and the $Sb_3F_{16}^-$ anion (F_1, −140.32 ppm (q); F_2, −112.18 ppm (dd); F_3, −89.66 ppm; F_4, −128.19 ppm (dt); F_5, −108.23 ppm (m); $^2J(F_1-F_2) = 57$ Hz; $^2J(F_2-F_3) = 99$ Hz; $^2J(F_3-F_4) = 37$ Hz; $^2J(F_4-F_5) = 134$ Hz); the numbering scheme of Gillespie et al. is used.[13,14] Abbreviations denote the following: singlet (s); doublet (d); quintet (q); multiplet (m); doublet of doublets (dd); doublet of triplets (dt); broad (br).

(13) Dean, P. A. W.; Gillespie, R. J. *J. Am. Chem. Soc.* **1969**, *91*, 7260.

(14) Bacon, J.; Dean, P. A. W.; Gillespie, R. J. *Can. J. Chem.* **1970**, *48*, 3413.

(15) Christe, K. O.; Dixon, D. A.; Mack, H. G.; Oberhammer, H.; Pagelot, A.; Sanders, J. C. P.; Schrobilgen, G. J. *J. Am. Chem. Soc.* **1993**, *115*, 11279.

Table 2. Experimental Bond Lengths (Å), Bond Angles (deg), and Contacts (Å) in $[OsO_3F][PnF_6]$ (Pn = As, Sb), and $[OsO_3F][HF]_2[AsF_6]$ and Calculated Geometries for $(FO_3Os\text{--}FPnF_5)_2$ and $(FO_3Os\text{--}(HF)_2\text{--}FAsF_5)_2$ at the LDFT and NLDFT Levels of Theory

	expt	calcd(LDFT)[a]	calcd(NLDFT)[b]		expt	calcd(LDFT)[a]	calcd(NLDFT)[b]
			$[OsO_3F][AsF_6]$				
Os(1)−O(1)	1.712(8)	1.700/1.700	1.715	Os(1)−O(2)	1.673(9)	1.698/1.698	1.713
Os(1)−O(3)	1.678(9)	1.702/1.703	1.718	Os(1)−F(1)	1.782(7)	1.854/1.855	1.879
Os(1)--F(2)	2.451(7)	2.288/2.287	2.417	Os(1)--F(4)	2.666(7)	2.289/2.289	2.293
Os(1)···F(5)	3.072(8)			As(1)−F(2)	1.776(7)	1.841/1.843	1.873
As(1)−F(3)	1.677(7)	1.728/1.729	1.759	As(1)−F(4)	1.746(7)	1.886/1.885	1.936
As(1)−F(5)	1.695(8)	1.734/1.736	1.763	As(1)−F(6)	1.685(8)	1.718/1.719	1.749
As(1)−F(7)	1.693(7)	1.732/1.733	1.764				
O(1)−Os(1)−O(2)	105.1(4)	105.2/105.3	105.0	O(1)−Os(1)−O(3)	108.4(4)	105.1/105.1	104.2
O(2)−Os(1)−O(3)	104.6(4)	101.6/101.6	102.5	O(1)−Os(1)−F(1)	120.4(4)	135.8/135.8	137.8
O(1)−Os(1)--F(2)	75.6(3)	80.3/80.3	78.8	O(2)−Os(1)−F(1)	105.6(4)	102.7/102.7	103.6
O(3)−Os(1)−F(1)	111.4(4)	101.9/101.9	99.0	O(2)−Os(1)--F(2)	179.0(4)	174.5/174.4	175.8
O(3)−Os(1)--F(2)	75.8(3)	76.2/76.2	78.0	F(1)−Os(1)--F(2)	73.5(3)	73.0/73.0	72.2
As(1)−F(2)--Os(1)	138.4(4)	134.4/134.3	145.0	F(2)−As(1)−F(3)	89.9(4)	86.5/86.4	87.0
F(2)−As(1)−F(4)	87.3(3)	83.8/83.8	84.0	F(2)−As(1)−F(5)	88.3(4)	87.1/87.1	87.3
F(2)−As(1)−F(6)	89.7(4)	89.2/89.2	90.4	F(2)−As(1)−F(7)	177.0(4)	174.5/174.4	172.9
F(3)−As(1)−F(4)	89.4(4)	85.1/85.1	84.8	F(3)−As(1)−F(5)	177.1(5)	168.8/168.7	169.7
F(3)−As(1)−F(6)	92.3(4)	94.7/94.7	94.4	F(3)−As(1)−F(7)	90.8(4)	92.9/92.9	92.5
F(4)−As(1)−F(5)	88.2(4)	85.1/85.1	86.1	F(4)−As(1)−F(6)	176.6(4)	173.0/173.0	174.3
F(4)−As(1)−F(7)	89.7(4)	90.7/90.6	88.9	F(5)−As(1)−F(6)	90.0(4)	94.4/94.4	94.1
F(5)−As(1)−F(7)	91.0(4)	92.6/92.6	92.1	F(6)−As(1)−F(7)	93.2(4)	96.4/96.4	96.7
F(2)--Os(1)--F(4A)	103.6(2)	98.9/99.0	93.7	F(1)−Os(1)--F(4A)	66.8(3)	71.5/71.5	72.1
O(2)−Os(1)--F(4)	76.0(3)	82.7/82.7	85.3	O(1)−Os(1)--F(4)	73.0(4)	79.0/79.0	80.1
			$[OsO_3F][SbF_6]$				
Os(1)−O(1)	1.708(7)	1.704/1.704	1.716	Os(1)−O(2)	1.681(8)	1.700/1.700	1.715
Os(1)−O(3)	1.696(7)	1.703/1.703	1.718	Os(1)−F(1)	1.844(6)	1.866/1.866	1.885
Os(1)--F(2)	2.236(6)	2.222/2.222	2.327	Os(1)--F(4)	2.315(6)	2.234/2.234	2.305
Sb(1)−F(2)	1.976(6)	1.841/1.843	2.046	Sb(1)−F(3)	1.845(6)	1.903/1.903	1.934
Sb(1)−F(4)	1.939(6)	2.039/2.039	2.070	Sb(1)−F(5)	1.846(6)	1.910/1.910	1.940
Sb(1)−F(6)	1.848(6)	1.902/1.902	1.933	Sb(1)−F(7)	1.846(6)	1.912/1.912	1.940
O(1)−Os(1)−O(2)	102.2(3)	105.2/105.3	103.8	O(1)−Os(1)−O(3)	102.8(3)	105.1/105.1	103.8
O(2)−Os(1)−O(3)	103.9(4)	101.6/101.6	103.3	O(1)−Os(1)−F(1)	145.0(3)	135.8/135.8	142.6
O(1)−Os(1)--F(2)	79.6(3)	80.3/80.3	79.9	O(2)−Os(1)−F(1)	97.5(3)	102.7/102.7	99.7
O(3)−Os(1)−F(1)	100.1(3)	101.9/101.9	98.4	O(2)−Os(1)--F(2)	167.4(3)	174.5/174.4	170.3
O(3)−Os(1)--F(2)	87.7(3)	76.2/76.2	84.3	F(1)−Os(1)--F(2)	75.3(2)	73.0/73.0	72.9
Sb(1)−F(2)--Os(1)	135.7(3)	134.4/134.3	144.7	F(2)−Sb(1)−F(3)	88.1(2)	86.5/86.4	85.5
F(2)−Sb(1)−F(4)	85.5(2)	83.8/83.8	85.4	F(2)−Sb(1)−F(5)	86.7(2)	87.1/87.1	86.6
F(2)−Sb(1)−F(6)	87.8(2)	89.2/89.2	87.2	F(2)−Sb(1)−F(7)	176.2(3)	174.5/174.4	176.2
F(3)−Sb(1)−F(4)	87.1(3)	85.1/85.1	83.9	F(3)−Sb(1)−F(5)	172.5(3)	168.8/168.7	164.5
F(3)−Sb(1)−F(6)	91.8(3)	94.7/94.7	96.6	F(3)−Sb(1)−F(7)	92.7(2)	92.9/92.9	94.3
F(4)−Sb(1)−F(5)	87.0(3)	85.1/85.1	82.2	F(4)−Sb(1)−F(6)	173.2(2)	173.0/173.0	172.6
F(4)−Sb(1)−F(7)	90.9(3)	90.7/90.6	90.7	F(5)−Sb(1)−F(6)	93.4(3)	94.4/94.4	96.4
F(5)−Sb(1)−F(7)	92.1(3)	92.6/92.6	92.7	F(6)−Sb(1)−F(7)	95.9(3)	96.4/96.4	96.6
F(2)−Os(1)--F(4A)	79.2(3)	98.9/99.0	84.5	F(1)−Os(1)--F(4A)	73.9(2)	71.5/71.5	72.4
O(2)−Os(1)--F(4)	88.9(3)	82.7/82.7	87.3	O(1)−Os(1)--F(4)	77.8(3)	79.0/79.0	80.0
			$[OsO_3F][HF]_2[AsF_6]$				
Os(1)−O(1)	1.694(6)	1.704/1.704	1.721/1.721	Os(1)−O(2)	1.669(6)	1.700/1.700	1.724/1.713
Os(1)−O(3)	1.719(6)	1.709/1.708	1.721/1.720	Os(1)−F(1)	1.804(5)	1.873/1.872	1.894/1.893
Os(1)--F(2)	2.282(5)	2.158/2.158	2.334/2.336	Os(1)--F(3)	2.231(4)	2.227/2.231	2.236/2.240
As(1)−F(3)	1.823(4)	1.886/1.887	1.963/1.964	As(1)−F(4)	1.735(5)	1.857/1.854	1.855/1.856
As(1)−F(5)	1.703(5)	1.738/1.737	1.767/1.767	As(1)−F(6)	1.696(5)	1.727/1.727	1.759/1.760
As(1)−F(7)	1.706(5)	1.732/1.732	1.762/1.762	As(1)−F(8)	1.690(5)	1.719/1.719	1.749/1.749
F(2)···F(9)	2.429(8)	2.298/2.298	2.388/2.389	F(9)···F(4)	2.512(8)	2.327/2.329	2.451/2.451
F(2)−H(1)		1.099/1.100	1.027/1.027	H(1)--F(9)		1.200/1.199	1.361/1.363
F(9)−H(2)		1.051/1.052	1.000/0.999	H(2)--F(4A)		1.283/1.280	1.457/1.458
O(1)−Os(1)−O(2)	103.0(3)	103.7/103.7	103.2/103.2	O(1)−Os(1)−O(3)	102.4(3)	103.4/103.5	103.0/103.2
O(2)−Os(1)−O(3)	103.5(3)	103.4/103.4	104.4/104.4	O(1)−Os(1)−F(1)	100.0(3)	97.3/97.4	96.0/95.9
O(2)−Os(1)−F(1)	101.2(3)	97.2/97.2	100.4/100.4	O(3)−Os(1)−F(1)	141.7(3)	146.1/146.0	144.1/144.0
O(2)−Os(1)--F(3)	87.5(2)	86.9/87.0	87.9/87.9	O(1)−Os(1)--F(3)	169.0(2)	167.1/167.1	166.3/166.3
O(3)−Os(1)--F(3)	78.2(2)	80.7/80.6	81.6/81.6	F(1)−Os(1)--F(3)	74.1(2)	73.8/73.8	73.8/73.8
O(2)−Os(1)--F(2)	169.1(2)	163.7/163.6	168.0/168.2	O(1)−Os(1)--F(2)	87.1(3)	90.4/90.7	86.6/86.4
O(3)−Os(1)--F(2)	78.0(2)	80.7/80.5	79.7/79.5	F(1)−Os(1)--F(2)	72.6(2)	72.6/72.7	71.3/71.4
F(3)--Os(1)--F(2)	82.3(2)	78.1/77.8	81.5/81.6	As(1)−F(3)--Os(1)	138.8(2)	124.9/124.2	131.2/130.7
F(3)−As(1)−F(4)	86.1(2)	83.8/83.9	84.0/83.8	F(3)−As(1)−F(5)	86.6(2)	86.7/86.3	86.3/86.2
F(3)−As(1)−F(6)	88.2(2)	88.3/88.1	87.6/87.8	F(3)−As(1)−F(7)	87.0(2)	84.7/84.9	84.1/84.2
F(3)−As(1)−F(8)	178.6(2)	174.2/174.6	175.7/175.6	F(4)−As(1)−F(5)	89.3(3)	85.2/85.5	86.5/86.7
F(4)−As(1)−F(6)	174.3(2)	172.0/172.0	171.6/171.6	F(4)−As(1)−F(7)	88.5(2)	86.0/85.7	87.0/87.0
F(4)−As(1)−F(8)	92.6(3)	90.5/90.8	91.8/91.8	F(5)−As(1)−F(6)	90.7(3)	93.2/93.6	92.1/92.2
F(5)−As(1)−F(7)	173.4(2)	168.3/168.2	169.0/169.1	F(5)−As(1)−F(8)	92.8(2)	93.6/93.5	94.5/94.5
F(6)−As(1)−F(7)	90.9(3)	94.4/94.1	92.9/92.8	F(6)−As(1)−F(8)	93.1(3)	97.4/97.2	96.6/96.6
F(7)−As(1)−F(8)	93.5(3)	94.2/94.4	94.7/94.6	F(9)−H(2)--F(4A)		172.5/172.8	171.6/171.6
H(2)−F(9)--H(1)		112.5/112.7	115.2/115.3	F(2)−H(1)--F(9)		177.2/177.0	178.2/178.3
Os(1)--F(2)−H(1)		121.2/121.3	121.4/121.8	As(1)−F(4)--H(2A)		121.2/119.0	122.7/123.1

[a] The two calculated values represent the distances and angles that are symmetry related in the crystal structure. [b] The two calculated distances and angles that are symmetry related in the crystal structure do not differ significantly.

Table 3. Experimental Bond Lengths (Å), Bond Angles (deg), and Contacts (Å) in $[OsO_3F][HF][SbF_6]$, and $[OsO_3F][Sb_3F_{16}]$

$[OsO_3F][HF][SbF_6]$					
Os(1)−O(12)	1.66(2)	Os(1)−O(13)	1.68(2)	Os(1)−O(11)	1.70(2)
Os(1)−F(11)	1.847(13)	Os(1)--F(13)	2.23(2)	Os(1)--F(12)	2.236(14)
Os(2)−O(21)	1.68(2)	Os(2)−O(23)	1.70(2)	Os(2)−O(22)	1.76(2)
Os(2)−F(21)	1.82(2)	Os(2)--F(23)	2.240(14)	Os(2)--F(22)	2.27(2)
Sb(1)−F(13)	1.96(2)	Sb(1)−F(14)	1.87(2)	Sb(1)−F(15)	1.86(2)
Sb(1)−F(16)	1.913(14)	Sb(1)−F(17)	1.85(2)	Sb(1)−F(18)	1.846(14)
Sb(2)−F(23)	1.977(14)	Sb(2)−F(24)	1.86(2)	Sb(2)−F(25)	1.850(14)
Sb(2)−F(26)	1.93(2)	Sb(2)−F(27)	1.87(2)	Sb(2)−F(28)	1.84(2)
F(12)···F(26)	2.38(2)				

O(11)−Os(1)−O(12)	103.1(9)	O(11)−Os(1)−O(13)	102.9(8)
O(11)−Os(1)−F(11)	101.2(8)	O(11)−Os(1)--F(12)	168.7(7)
O(11)−Os(1)--F(13)	87.1(8)	O(12)−Os(1)−O(13)	103.8(8)
O(12)−Os(1)−F(11)	98.0(7)	O(12)−Os(1)--F(12)	87.4(7)
O(12)−Os(1)--F(13)	167.8(7)	O(13)−Os(1)−F(11)	142.7(7)
O(13)−Os(1)--F(12)	78.2(7)	O(13)−Os(1)--F(13)	80.1(7)
F(11)−Os(1)--F(12)	72.9(5)	F(11)−Os(1)--F(13)	73.1(5)
F(12)−Os(1)--F(13)	82.0(5)	O(21)−Os(2)−O(22)	101.4(9)
O(21)−Os(2)−O(23)	102.7(9)	O(21)−Os(2)−F(21)	100.0(8)
O(21)−Os(2)--F(22)	87.5(7)	O(21)−Os(2)--F(23)	170.1(7)
O(22)−Os(2)−O(23)	102.4(9)	O(22)−Os(2)−F(21)	143.4(8)
O(22)−Os(2)--F(22)	77.9(7)	O(22)−Os(2)--F(23)	79.8(7)
O(23)−Os(2)−F(21)	101.3(8)	O(23)−Os(2)--F(22)	169.5(7)
O(23)−Os(2)--F(23)	86.5(7)	F(21)−Os(2)--F(22)	73.8(7)
F(21)−Os(2)--F(23)	74.3(6)	F(23)--Os(2)--F(22)	83.2(5)
Sb(1)−F(13)--Os(1)	151.8(7)	Sb(2)−F(23)--Os(2)	137.7(7)
F(13)−Sb(1)−F(18)	179.2(6)	F(13)−Sb(1)−F(17)	86.5(6)
F(13)−Sb(1)−F(15)	89.1(6)	F(13)−Sb(1)−F(14)	87.8(7)
F(13)−Sb(1)−F(16)	87.1(6)	F(23)−Sb(2)−F(28)	175.1(6)
F(23)−Sb(2)−F(25)	86.4(6)	F(23)−Sb(2)−F(24)	88.1(6)
F(23)−Sb(2)−F(27)	85.3(6)	F(23)−Sb(2)−F(26)	84.6(6)

$[OsO_3F][Sb_3F_{16}]$					
Os(1)−FOA	1.68(3)	Sb(1)−F(2)	1.84(4)	Sb(1)−F(1)	1.87(3)
Sb(1)−F(3)	1.88(4)	F(1)−Sb(2)	2.19(3)	Sb(2)−F(10A)	1.77(6)
Sb(2)−F(12)	1.78(4)	Sb(2)−F(11B)	1.80(5)	Sb(2)−F(10B)	1.87(6)
Sb(2)−F(11A)	1.91(5)	Os(1)···F(10A)	2.85(6)	Os(1)···F(10B)	2.83(6)

FOA#1−Os(1)−OFA	104(2)	OFA−Os(1)−FOA#2	112.5(10)
F(1)−Sb(1)−F(2)	85(2)	F(1)−Sb(1)−F(3)	90.8(14)
F(2)−Sb(1)−F(3)	78(2)	Sb(1)−F(1)−Sb(2)	146(2)
F(1)−Sb(2)−F(10B)	81(2)	F(1)−Sb(2)−F(11A)	83(2)
F(1)−Sb(2)−F(12)	173.8(14)	F(1C)−Sb(2)−F(10A)	87(2)
F(1C)−Sb(2)−F(11B)	91(2)		

OOO face, such that they are located on the sides opposite to the Os−O bonds. Extension of the coordination sphere to include the Os···F secondary contacts results in a monocapped octahedral geometry about Os in which the three oxygen atoms are cis to one another (Figure 1). The longer Os−O(1) bond is opposite to the longest Os···F contact and is likely a consequence of the steric crowding caused by the two short Os--F contacts in the vinicity of O(1). The short Os--F contacts join two anions and two cations to form a cyclic $(FO_3Os\text{--}FAsF_5)_2$ dimer having two short contacts (2.450(7) Å) and two longer contacts (2.666(7) Å). This contrasts with the four nearly equivalent and shorter Os--F contacts (2.287 to 2.289 Å) found in the fully optimized LDFT gas-phase geometry of this dimer (see Computational Results, part c). The NLDFT geometry optimization gives better agreement with the experimental geometry but gives a less pronounced difference in the Os--F contacts (2.293 and 2.417 Å) than the experimental geometry. Two *cis*-fluorines of the AsF_6^- anion form two strong contacts to the cation resulting in elongation of both As−F bonds (1.776(7) and 1.746(7) Å) relative to the four remaining As−F bonds (1.695(8)−1.677(7) Å) and in lowering of the anion point symmetry to C_{2v} or lower.

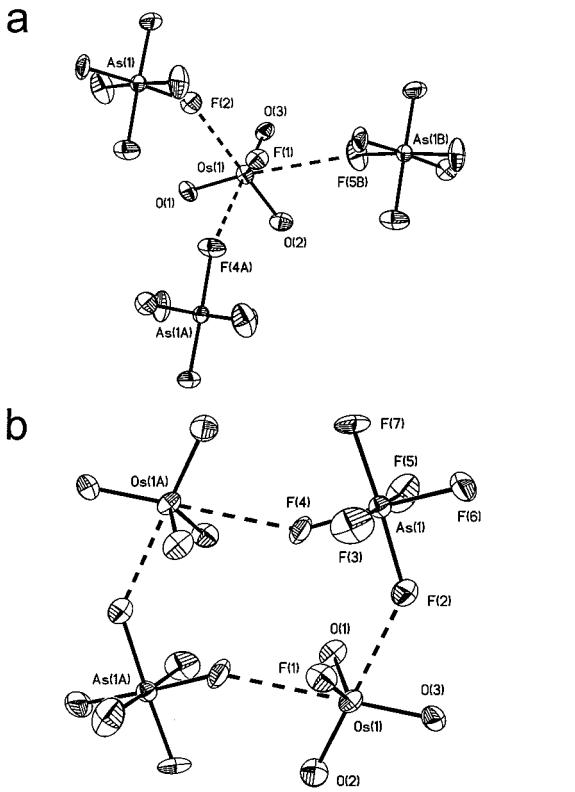

Figure 1. Views of (a) the OsO_3F^+ cation and its contacts with AsF_6^- anions in the $[OsO_3F][AsF_6]$ structure and (b) the $([OsO_3F][AsF_6])_2$ dimer. Thermal ellipsoids are shown at the 50% probability level.

(b) $[OsO_3F][SbF_6]$. The structure of $[OsO_3F][SbF_6]$ consists of fluorine-bridged $(FO_3Os\text{--}FSbF_5)_2$ dimers (Figure 10, Supporting Information), as found in the structure of $[OsO_3F][AsF_6]$. The coordination number of osmium is expanded to 6 with a facial OsO_3F_3 arrangement. The distortion of the OsO_3F^+ cation from the expected C_{3v} point symmetry is more pronounced in $[OsO_3F][SbF_6]$ than in the AsF_6^- salt, which is a consequence of the two shorter Os--F contacts (2.236(6) and 2.315(6) Å) in the SbF_6^- compound, and results in significant elongation of the Os(1)−F(1) bond (1.844(6) Å) when compared with that of the AsF_6^- analogue (1.782(7) Å). As a consequence of the stronger Os--F contacts, the F(1)−Os(1)−O(1) angle in $[OsO_3F][SbF_6]$ (145.0(3)°) is more open and the F(1)−Os(1)−O(2)/O(3) angles (97.5(3)/100.1(3)°) are more closed than in $[OsO_3F]$-$[AsF_6]$. The shorter Os--F contacts in the crystal structure of $[OsO_3F][SbF_6]$ compared with those in $[OsO_3F][AsF_6]$ are in good agreement with the calculated values for the $(FO_3Os\text{--}FPnF_5)_2$ dimers (see Computational Results, part c).

(c) $[OsO_3F][HF]_2[AsF_6]$. The crystal structure of $[OsO_3F][HF]_2[AsF_6]$ consists of cyclic dimers comprising two AsF_6^- anions fluorine bridged to the OsO_3F^+ cations which are, in turn, bridged through two hydrogen bonded $(HF)_2$ moieties to a second cation−anion pair (Figure 2). These cyclic dimers, aligned parallel to the $(10^1/_2)$ plane, are located on a cystallographic inversion center and are stacked in columns parallel to the *a* axis (Figure 11, Supporting Information).

The OsO_3F^+ cation deviates significantly from the ideal C_{3v} structure with one short (1.666(6) Å) and two long

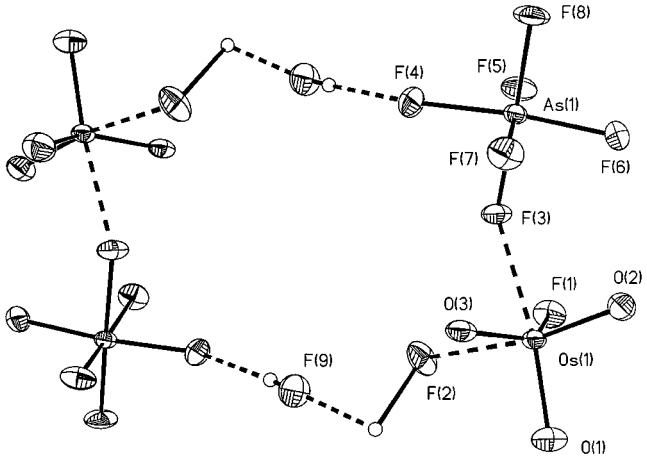

Figure 2. View of the $([OsO_3F][HF]_2[AsF_6])_2$ dimer structural unit. Thermal ellipsoids are shown at the 50% probability level.

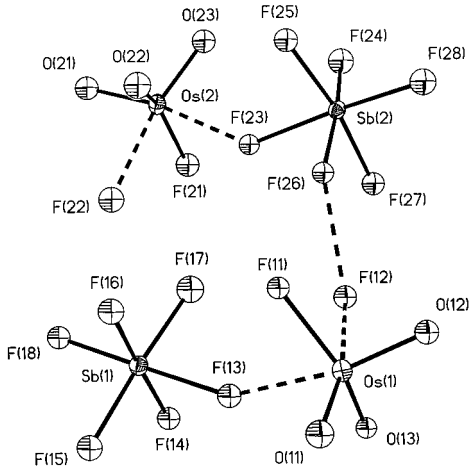

Figure 3. View of the asymmetric unit of $[OsO_3F][HF][SbF_6]$. Thermal ellipsoids are shown at the 50% probability level. The hydrogen atoms of coordinated HF molecules were not refined and are, therefore, not shown.

(1.694(6) and 1.704(6) Å) Os−O bonds. The Os−F bond length in the cation (1.804(5) Å) is similar to that in $[OsO_3F][AsF_6]$ (1.787(7) Å); however, unlike the latter structure and similar to the $[OsO_3F][SbF_6]$ structure, the O−Os−F bond angles in $[OsO_3F][HF]_2[AsF_6]$ (100.0(3), 102.4(3), and 141.6(3)°) are significantly distorted from the ideal C_{3v} symmetry of the free OsO_3F^+ cation as a result of secondary contacts with one fluorine from an AsF_6^- anion and one fluorine from an HF solvent molecule. The resulting OsO_3F_3 moiety resembles the facial arrangement of the oxygen and fluorine atoms found for the *fac*-$OsO_3F_3^-$ anion in $[N(CH_3)_4][OsO_3F_3]$.[4] The Os--F contacts (2.230(4) and 2.279(5) Å) are similar to those found in $[OsO_3F][SbF_6]$ but are much shorter than those in $[OsO_3F][AsF_6]$ (2.450(7) Å). This structure, together with that of $[OsO_3F][HF][SbF_6]$ (vide infra), represent rare examples of HF molecules coordinated to metal centers. The only other reported examples are $[La][HF]_2[AsF_6]_3$[16] and $[(\eta^5\text{-}C_5Me_5)NbF_4(HF)AsF_3]_2$.[17] In the latter structure, HF also bridges two metal centers. The F(2)···F(9) and F(9)···F(4A) distances in $[OsO_3F][HF]_2[AsF_6]$ are 2.429(8) and 2.512(8) Å, respectively, and are shorter than the F···F distance in $[(\eta^5\text{-}C_5Me_5)NbF_4(HF)AsF_3]_2$ (2.686 Å),[17] indicating stronger hydrogen-bonding interactions in the $[OsO_3F][HF]_2[AsF_6]$ structure. The F···F distances in $[OsO_3F][HF]_2[AsF_6]$ are, however, significantly greater than that found for bifluoride in $[N(CH_3)_4][HF_2]$ (2.213(4) Å)[18] and are also significantly greater than the F···F distances in *trans*-$[Ru(dmpe)_2(H)(FHF)]$ (2.276(8) Å),[19] *trans*-$Pd(PPh_3)_2Me(FHF)$ (2.31 Å),[20] $Mo(PMe_3)_4(H)_2F(FHF)$ (2.351(8) Å),[21] $WF(H)_2(FHF)(PMe_3)_4$ (2.389(6) Å),[22] and $NiF(HF)(C_4N_2F_2H)(PEt_3)_2$ (2.400(6) Å),[23] where one HF molecule is hydrogen-bridged to a fluorine ligand of the metal center. The previously reported structures, however, contain a terminal HF molecule and can, alternatively, be described as an HF_2^- ligand coordinated to the metal.

The symmetry of the AsF_6^- anion is lowered to C_{2v} point symmetry or lower by formation of As−F--Os and As−F--HF bridges, which are cis to one another, producing significantly elongated As−F bonds of 1.823(4) and 1.735(5) Å, respectively, when compared with the remaining four As−F bonds (1.689(4)−1.705(5) Å).

(d) $[OsO_3F][HF][SbF_6]$. The $[OsO_3F][HF][SbF_6]$ salt crystallizes in the noncentrosymmetric *Pc* space group as a 2:1 twin preventing a proper absorption correction. As a consequence, it was not possible to refine the fluorine and oxygen atoms anisotropically. The relatively large errors in the bond lengths and bond angles prevented a detailed comparison with related structures. Two fluorine-bridged OsO_3F^+/SbF_6^- ion pairs were defined in the asymmetric unit (Figure 3). One HF molecule bridges the osmium center and a fluorine of the SbF_6^- anion of another OsO_3F^+/SbF_6^- ion pair, resulting in a helical arrangement comprised of alternating OsO_3F^+ and SbF_6^- ions running parallel to the *a* axis (Figure 12, Supporting Information). The bond lengths and angles in both crystallographically independent anion−cation pairs are the same within 3σ.

All metric parameters involving osmium in $[OsO_3F][HF][SbF_6]$ are the same, within 3σ, as those in $[OsO_3F][HF]_2[AsF_6]$. As in the case of $[OsO_3F][HF]_2[AsF_6]$, the primary coordination sphere of the OsO_3F^+ cation is expanded to six by fluorine bridge formation with an SbF_6^- anion and an HF molecule, resulting in *fac*-OsO_3F_3 coordination. One F−Os−O bond angle of the OsO_3F^+ cation is also significantly larger (142.7(7)/143.4(8)°) than the remaining two angles (98.0(7)/100.0(8) and 101.2/101.3(8)°).

(e) $[OsO_3F][Sb_3F_{16}]$. The crystal structure of $[OsO_3F][Sb_3F_{16}]$ consists of well-separated OsO_3F^+ cations and *cis*-

(16) Mazej, Z.; Borrmann, H.; Lutar, K.; Žemva, B. *Inorg. Chem.* **1998**, *37*, 5912.
(17) Roesky, H. W.; Sotoodeh, M.; Xu, Y. M.; Schrumpf, F.; Noltemeyer, M. *Z. Anorg. Allg. Chem.* **1990**, *580*, 131.
(18) Wilson, W. W.; Christe, K. O.; Feng, J.-a.; Bau, R. *Can. J. Chem.* **1989**, *67*, 1898.
(19) Whittlesey, M. K.; Perutz, R. N.; Greener, B.; Moore, M. H. *J. Chem. Soc., Chem. Commun.* **1997**, 187.
(20) Roe, D. C.; Marshall, W. J.; Davidson, F.; Soper, P. D.; Grushin, V. V. *Organometallics* **2000**, *19*, 4575.
(21) Murphy, V. J.; Hascall, T.; Chen, J. Y. Parkin, G. *J. Am. Chem. Soc.* **1996**, *118*, 7428.
(22) Murphy, V. J.; Rabinovich, D.; Hascall, T.; Klooster, W. T.; Koetzle, T. F.; Parkin, G. *J. Am. Chem. Soc.* **1998**, *120*, 4372.
(23) Braun, T.; Foxon, S. P.; Perutz, R. N.; Walton, P. H. *Angew. Chem.* **1999**, *38*, 3326; *Angew. Chem., Int. Ed. Engl.* **1999**, *111*, 3543.

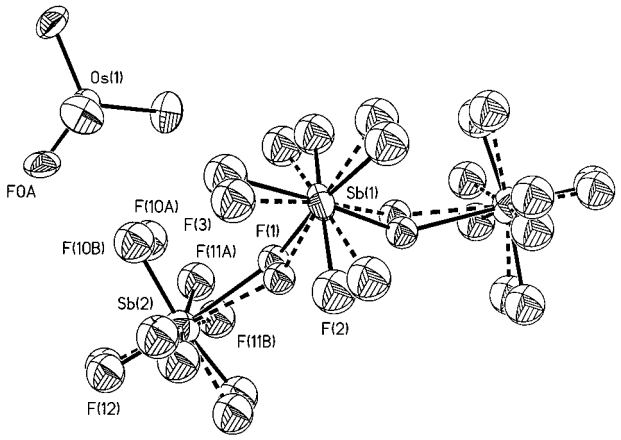

Figure 4. View of the OsO_3F^+ and $Sb_3F_{16}^-$ ions. Thermal ellipsoids are shown at the 50% probability level.

fluorine-bridged $Sb_3F_{16}^-$ anions. The OsO_3F^+ cation is located on a special position ($\bar{4}$..) resulting in a positional disorder of the symmetry-related oxygen and fluorine atoms. A disorder between two different orientations was resolved for the $Sb_3F_{16}^-$ anion (Figure 4). The disorders in the cation and anion prevented the anisotropic refinement of all the fluorine and oxygen atoms, giving rise to a relatively large R factor. The *cis*-fluorine-bridged $Sb_3F_{16}^-$ anions pack in the (110) and ($\bar{1}$10) planes in such a way that they form square-based channels parallel to the *c* axis that are filled with rows of OsO_3F^+ cations (Figure 13, Supporting Information). The first coordination sphere around osmium is essentially tetrahedral with an average Os−O/F bond length of 1.68(3) Å, which is the same as the average of the Os−O and Os−F bond lengths in $[OsO_3F][AsF_6]$, $[OsO_3F][SbF_6]$, $[OsO_3F][HF]_2[AsF_6]$, and $[OsO_3F][HF][SbF_6]$. The osmium atom also has long contacts to a fluorine of each of four $Sb_3F_{16}^-$ anions (Os···F(10B/10A); 2.83(6)/2.85(6) Å) with a trajectory through the center of each trigonal face of the tetrahedral cation, giving rise to a second tetrahedral coordination sphere. The $Sb_3F_{16}^-$ anion adopts a *cis*-fluorine-bridged geometry, as found for the $Sb_3F_{16}^-$ and $Sb_4F_{21}^-$ anions in the crystal structures of $[XeN(SO_2F)_2][Sb_3F_{16}]$,[24] $[OCNCO][Sb_3F_{16}]$,[25] $[Cl_3][Sb_3F_{16}]$,[26] and $[Xe_2][Sb_4F_{21}]$,[27] respectively. This geometry was also found in SO_2ClF solutions of $[OsO_3F][Sb_3F_{16}]$ by ^{19}F NMR spectroscopy and contrasts with the structure of $[Br_2][Sb_3F_{16}]$ in which $Sb_3F_{16}^-$ was found to contain a *trans*-fluorine-bridged $Sb_3F_{16}^-$ anion.[28] The high standard deviations in the bond lengths and bond angles of the $Sb_3F_{16}^-$ anion prevent detailed comparisons with related anion structures.

Raman Spectroscopy. The $[OsO_3F][Sb_3F_{16}]$, $[OsO_3F][PnF_6]$ (Pn = As, Sb), $[OsO_3F][HF][SbF_6]$, $[OsO_3F][HF]_2[PnF_6]$ (Pn = As, Sb), and $[\mu$-$F(OsO_3F)_2][AsF_6]$ salts were characterized by low-temperature Raman spectroscopy (Figures 5−8), and the observed Raman frequencies and their assignments are given in Tables 4−8. The free OsO_3F^+ cation is expected to have C_{3v} point symmetry with the vibrational modes spanning the irreducible representations $3A_1 + 3E$, where all modes are infrared and Raman active. The vibrational assignments are based on the frequencies and assignments derived from DFT calculations (see Computational Results) and are also listed in Tables 4−8.

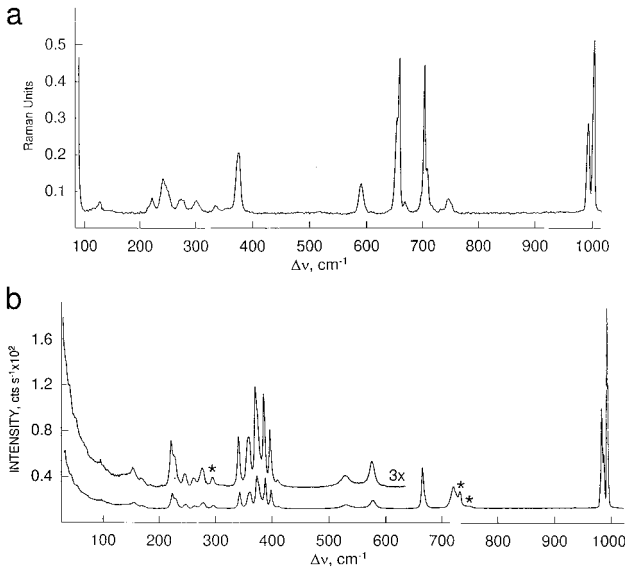

Figure 5. Raman spectra of (a) microcrystalline $[OsO_3F][Sb_3F_{16}]$ recorded in a Pyrex glass capillary at −165 °C using 1064-nm excitation and (b) microcrystalline $[OsO_3F][AsF_6]$ recorded in a $^1/_4$-in. FEP sample tube at −150 °C using 647.1-nm excitation. Asterisks (*) denote FEP sample tube lines.

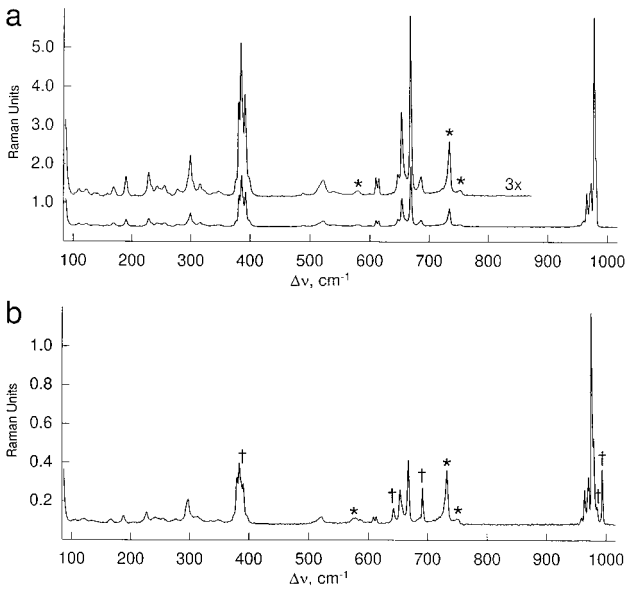

Figure 6. Raman spectra recorded in $^1/_4$-in. FEP sample tubes using 647.1-nm excitation: (a) microcrystalline $[OsO_3F][HF][SbF_6]$ at −165 °C; (b) microcrystalline $[OsO_3F][HF][SbF_6]$ containing $[OsO_3F][SbF_6]$ at −150 °C. Asterisks (*) denote FEP sample tube lines and daggers (†) denote bands arising from $[OsO_3F][SbF_6]$.

(a) $[OsO_3F][Sb_3F_{16}]$. The low-temperature Raman spectrum of $[OsO_3F][Sb_3F_{16}]$ contains six bands attributed to the OsO_3F^+ cation and anion bands in the Sb−F stretching and

(24) Faggiani, R.; Kennepohl, D. K.; Lock, C. J. L.; Schrobilgen, G. J. *Inorg. Chem.* **1986**, *25*, 563.
(25) Bernhardi, I.; Drews, T.; Seppelt, K. *Angew. Chem.* **1999**, *111*, 2370; *Angew. Chem., Int. Ed. Engl.* **1999**, *38*, 2232.
(26) Drews, T.; Koch, W.; Seppelt, K. *J. Am. Chem. Soc.* **1999**, *121*, 4379.
(27) Drews, T.; Seppelt, K. *Angew. Chem.* **1997**, *109*, 264; *Angew. Chem., Int. Ed. Engl.* **1997**, *36*, 273.
(28) Edwards, A. J.; Jones, G. R.; Sills, R. J. *J. Chem. Soc., Chem. Commun.* **1968**, 1527.

Table 4. Experimental Raman Frequencies for $[OsO_3F][Sb_3F_{16}]$ and Calculated Vibrational Frequencies for OsO_3F^+ and ReO_3F and Their Assignments

freq, cm^{-1}					
OsO_3F^+			ReO_3F		assgnt: MO_3F (C_{3v}) M = Os, Re
obsd[a,b]	calcd[c](LDFT)	calcd(NLDFT)	obsd[d]	calcd[c](LDFT)	
1002(100)	1038(4)	998(4)	1017.5	1032(15)	$\nu_1(A_1)$, $\nu_s(MO_3)$
992(53)	1024(81)	984(75)	983	998(271)	$\nu_4(E)$, $\nu_{as}(MO_3)$
745(9)	755(47)	715(45)	701	712(86)	$\nu_2(A_1)$, $\nu_s(MF)$
372(36)	346(0)	336(0)	354	338(2)	$\nu_5(E)$, $\delta_{as}(MO_3)$
333(4)	305(1)	295(1)	318.5	294(7)	$\nu_3(A_1)$, $\delta_s(MO_3)$
238(21)	224(4)	217(4)	237	222(4)	$\nu_6(E)$, δ(FMO)
731(3)					
707(25)					
701(87)					
696(10), sh					$Sb_3F_{16}^-$, ν(SbF)
666(7)					
656(92)					
652(56)					
588(18)					
298(7)					
271(9)					
248(13)					
242(16)					
218(9)					
212(3)					$Sb_3F_{16}^-$, δ(SbF)
125(6)					
84(86)					
71(7)					
60(6)					

[a] Spectrum recorded on the microcrystalline solid in a Pyrex glass capillary at −165 °C using 1064-nm excitation. Abbreviation (sh) denotes a shoulder. [b] Values in parentheses denote relative experimental Raman intensities. [c] Infrared intensities in km mol^{-1} are given in parentheses. [d] Infrared frequencies from a N_2 matrix; data from ref 8.

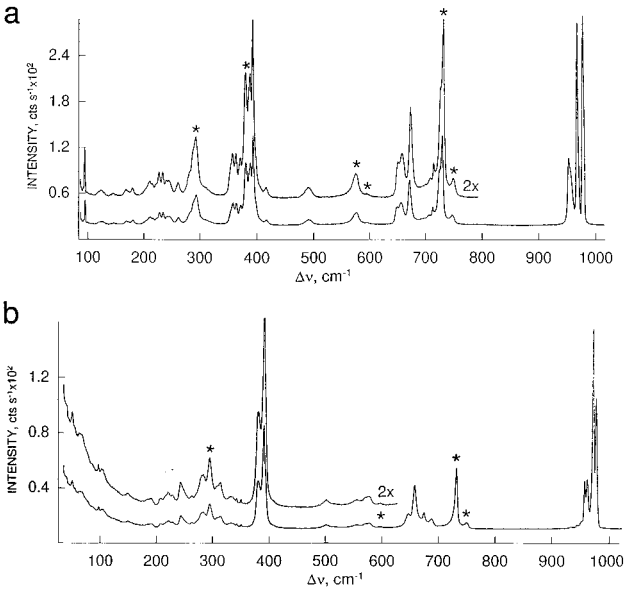

Figure 7. Raman spectra recorded in 1/4-in. FEP sample tubes using 647.1-nm excitation: (a) microcrystalline $[OsO_3F][HF]_2[AsF_6]$ at −140 °C; (b) microcrystalline $[OsO_3F][HF]_2[SbF_6]$ under HF solvent at −80 °C. Asterisks (*) denote FEP sample tube lines.

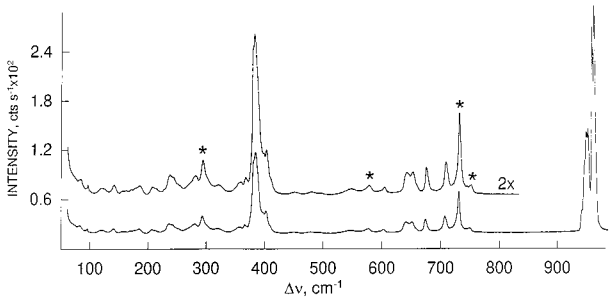

Figure 8. Raman spectra of microcrystalline $[\mu\text{-}F(OsO_3F)_2][AsF_6]$ under HF solvent recorded in a 1/4-in. FEP sample tube at −80 °C using 647.1-nm excitation. Asterisks (*) denote FEP sample tube lines.

F−Sb−F bending regions. The frequencies and intensities of the Raman bands for the $Sb_3F_{16}^-$ anion reported in the literature vary significantly depending on the nature of the countercation. Among the five known $Sb_3F_{16}^-$ salts that have been characterized by Raman spectroscopy, i.e., [ClCO]-$[Sb_3F_{16}]$,[29] [OCNCO]$[Sb_3F_{16}]$,[25] $[PF_4][Sb_3F_{16}]$,[30] $[XeN(SO_2F)_2]$-$[Sb_3F_{16}]$,[24] and $[ReF_6][Sb_3F_{16}]$,[31] the Raman frequencies and intensities attributed to the $Sb_3F_{16}^-$ anion in $[PF_4][Sb_3F_{16}]$ show the best agreement with those of $[OsO_3F][Sb_3F_{16}]$.

The Raman frequencies of the OsO_3F^+ cation agree well with those calculated using DFT calculations. The presence of only two Os−O stretching bands ($\nu_1(A_1)$ and $\nu_4(E)$) is consistent with the C_{3v} point symmetry of the OsO_3F^+ cation and is confirmed by the high symmetry of the disordered cation in the crystal structure of $[OsO_3F][Sb_3F_{16}]$ (see X-ray Crystallography, part c). The Os−O stretches of the OsO_3F^+ cation (992, 1002 cm^{-1}) appear at significantly higher frequencies than those of the matrix-isolated neutral parent molecule, monomeric OsO_3F_2 (929.0, 946.5 cm^{-1}),[32] which is in accord with stronger and less polar Os−O bonds. The Re−O stretching frequencies of isoelectronic ReO_3F agree

(29) Christe, K. O.; Hoge, B.; Boatz, J. A.; Prakash, G. K. S.; Olah, G. A.; Sheehy, J. A. *Inorg. Chem.* **1999**, *38*, 3132.
(30) Chen, G. S. H.; Passmore, J. *J. Chem. Soc., Dalton Trans.* **1979**, 1251.
(31) Schrobilgen, G. J.; Holloway, J. H.; Russell, D. R.; *J. Chem. Soc., Dalton Trans.* **1984**, 1411.
(32) Beattie, I. R.; Blayden, H. E.; Crocombe, R. A.; Jones, P. J.; Ogden, J. S. *J. Raman Spectrosc.* **1976**, *4*, 313.

Table 5. Raman Frequencies and Their Assignments for $[OsO_3F][PnF_6]$ (Pn = As, Sb)

$[OsO_3F][AsF_6]$[a]			$[OsO_3F][SbF_6]$[b]		
freq, cm^{-1}			freq, cm^{-1}		
obsd[c]	calcd[d](NLDFT)	assgnt	obsd[c]	calcd[d](NLDFT)	assgnt
	972(38)	Os−O stretches		969(42)	Os−O stretches
996(100)	971(4)		995(100)	969(0)	
	962(123)			960(136)	
990(27)	961(2)		986(32)	959(0)	
	958(168)			957(165)	
986(50)	957(0)			957(0)	
984(14), sh					
	709(233)	As−F stretches	692(65)	638(0)	Sb−F stretches
725(8), sh	706(0)			637(56)	
	685(308)			652(185)	Os−F stretches
721(11)	684(0)		656 sh	648(0)	
	660(237)	As−F + Os−F stretches		625(198)	Sb−F stretches
666(21)	656(0)		642(28)	624(0)	
	654(82)			606(174)	
	652(0)			605(0)	
	606(27)	As−F stretches		572(11)	
576(5)	606(0)			572(0)	
	499(253)	As−F−Os bridging stretches		493(279)	Sb−F−Os bridging stretches
529(2)	498(0)			492(0)	
	446(158)			462(186)	
410(1)	429(0)			442(0)	
397(10)	376(0)			372(0)	
	376(5)			371(6)	
387(16)	369(0)			368(11)	
	367(25)		386 sh	368(0)	
374(13), sh	359(0)			362(0)	
372(17)	353(6)			362(12)	
	351(92)			308(43)	
358(8)	349(0)			301(0)	
	341(114)			276(0)	
341(8)	338(0)			272(0)	
	329(87)			267(68)	
276(3)	327(0)			265(86)	
	318(7)			253(136)	
259(2)	318(0)			251(0)	
	313(0)			249(0)	
	311(65)			247(29)	
	300(7)			232(0)	
244(3)	299(0)			231(6)	
	264(45)			231(34)	
225(5)	243(0)			222(44)	
	232(14)			222(0)	
221(8)	230(0)			209(0)	
	230(68)			194(0)	
	223(0)			192(10)	
	211(0)			174(0)	
	200(14)			167(16)	
	191(0)			157(6)	
	187(33)			155(0)	
	171(1)			146(19)	
167(1)	154(0)			143(0)	
	150(12)			136(9)	
152(3)	139(0)			122(0)	
	131(0)			108(0)	
	126(5)			102(1)	
	116(0)			95(19)	
	109(5)			94(0)	
	104(18)			90(3)	
	78(0)			73(0)	
	74(9)			60(0)	
	64(0)			58(6)	
	49(0)			54(0)	
	47(0)			44(1)	
	36(0)			39(1)	
	34(0)			32(0)	
	22(1)			9(0)	
	19(0)			0(0)	
				−24(1)	

[a] Spectrum recorded on the microcrystalline solid in a $^1/_4$-in. FEP sample tube at −150 °C using 647.1-nm excitation. Bands arising from the FEP sample tube were observed at 293 (2), 733 (9), and 746 (2) cm^{-1}. [b] Spectrum recorded on the solid in admixture with $[OsO_3F][HF][SbF_6]$ in a $^1/_4$-in. FEP sample tube at −165 °C using 1064-nm excitation. [c] Values in parentheses denote relative Raman intensities. Abbreviation (sh) denotes a shoulder. [d] Vibrational frequencies were calculated for the optimized (NLDFT) structures of the $(FO_3Os\text{--}FPnF_5)_2$ dimers. Infrared intensities in km mol^{-1} are given in parentheses.

Table 6. Raman Frequencies and Their Assignments for $[OsO_3F][HF][SbF_6]$

freq,[a] cm^{-1}	assgnt OsO_3F^+ (C_{3v})	assgnt SbF_6^- (C_{4v})
981(33)	$\nu_s(OsO_3)$	
977(100)		
972(21)	$\nu_{as}(OsO_3)$	
970(17)		
965(16)	$\nu_{as}(OsO_3)$	
960(3)		
685(3)		$\nu_8(E)$
668(29)		$\nu_1(A_1)$
652(13)	$\nu_s(OsF)$	
645(3)		$\nu_2(A_1)$
613(3)		
609(3)		$\nu_5(B_1)$
537(1)		
520(3)		
515(2) sh		
487(<0.5)		$\nu_4(A_1)$
397(3)		
390(17)		
384(25)	$\delta_s(OsO_3)$	
380(16)		
375(3)		
345(<0.5)		
312(2)		
297(6)[b]		$\nu_9(E)$
275(1)		
254(2)		
239(1)		
226(4)		
187(3)		
165(1)		
155(<0.5)		
135(<0.5)		
120(1)		
106(1)		

[a] Spectrum recorded on the microcrystalline solid in a $^1/_4$-in. FEP sample tube at −150 °C using 1064-nm excitation. Values in parentheses denote relative intensities. Abbreviation (sh) denotes a shoulder. Bands arising from the FEP sample tube were observed at 297 (6), 579 (1), 734 (8), and 751 (1) cm^{-1}, and a laser line at 84 (12) cm^{-1} was observed. [b] This band overlaps with a band arising from the FEP sample tube.

well with those of the cationic Os analogue and differ by less than 15 cm^{-1}. The Raman band at 745 cm^{-1} is assigned to the Os−F stretch, which is at significantly higher frequency than those of the matrix-isolated OsO_3F_2 monomer (619.0, 646.0 cm^{-1})[32] and ReO_3F (701 cm^{-1})[8] and is in accord with the positive charge on OsO_3F^+ and a correspondingly less polar Os−F bond. The asymmetric OsO_3 bend appears at 370 cm^{-1}, which is between the ReO_3 bending frequencies in ReO_3F obtained from an HF solution (403 cm^{-1})[7] and that determined in a N_2 matrix (354 cm^{-1}).[9] The ordering of the asymmetric (ν_5(E)) and symmetric ($\nu_2(A_1)$) bends, although counterintuitive considering the significantly greater Raman intensity of the ν_5(E) band, is based on the DFT calculations and on previous assignments for ReO_3F[9,33] and TcO_3F.[33]

The $[OsO_3F][Sb_3F_{16}]$ salt represents the best approximation to a free OsO_3F^+ cation as evidenced by the absence of splitting for the degenerate modes of OsO_3F^+ and the fact that the stretching modes appear at the highest frequencies when compared with those of other OsO_3F^+ salts (vide infra).

(b) $[OsO_3F][AsF_6]$ and $[OsO_3F][SbF_6]$. The Raman spectrum of $[OsO_3F][AsF_6]$ is far more complex than suggested by its simple ionic formulation. The observation of 23 bands indicates a significant reduction of symmetry from the ideal C_{3v} point symmetry of the OsO_3F^+ cation and O_h symmetry of the AsF_6^- anion and is corroborated by the crystallographic findings. The Raman frequencies of only the most intense bands of $[OsO_3F][SbF_6]$ have been observed because $[OsO_3F][SbF_6]$ could only be obtained as a minor component in admixture with $[OsO_3F][HF][SbF_6]$ (vide supra). The Os−O stretching bands of $[OsO_3F][SbF_6]$ are, however, in excellent agreement with those of the AsF_6^- salt.

The Os−O stretching frequencies in $[OsO_3F][AsF_6]$ are approximately 6 cm^{-1} lower than those in $[OsO_3F][Sb_3F_{16}]$ resulting from the higher nucleophilicity of the AsF_6^- anion, which forms stronger fluorine bridge contacts to the OsO_3F^+ cation in the solid state to give the $(FO_3Os\text{--}FAsF_5)_2$ dimer (see X-ray Crystallography, part a). These contacts distort the OsO_3F^+ cation from C_{3v} symmetry, resulting in the splitting of the doubly degenerate Os−O stretching mode and the observation of three Os−O stretching bands. A shoulder at 984 cm^{-1} is assigned to the in-phase, out-of-phase coupling of the OsO_3 modes in the dimer. The assignments of the bands are based on the calculated frequencies at the NLDFT level of theory (see Computational Results and Table 4) and the rule of mutual exclusion of Raman and infrared bands, which should hold for the centrosymmetric $(FO_3Os\text{--}FAsF_5)_2$ dimer. On the basis of the calculated vibrational frequencies and comparisons with vibrational spectra of [NgF][AsF_6] (Ng = Kr, Xe),[34,35] the Os−F stretching mode in $[OsO_3F][AsF_6]$ was distinguished from the As−F stretching modes and is tentatively assigned to the band at 666 cm^{-1}, which is significantly lower than those of $[OsO_3F][Sb_3F_{16}]$ (745 cm^{-1}) and $[Os_2O_6F_3][AsF_6]$ (708 cm^{-1}). Detailed assignments of the low-frequency modes are not given because strong vibrational couplings among these modes result in complex descriptions of their motions.

(c) $[OsO_3F][HF]_2[PnF_6]$ (Pn = As, Sb) and $[OsO_3F][HF][SbF_6]$. As in the case of $[OsO_3F][AsF_6]$, the Raman spectra of $[OsO_3F][HF]_2[PnF_6]$ and $[OsO_3F][HF][SbF_6]$ indicate lowering of the cation and anion symmetries from their respective ideal C_{3v} and O_h point symmetries. The SbF_6^- anion bands in $[OsO_3F][HF][SbF_6]$ were assigned under C_{4v} point symmetry on the basis of previous assignments;[34,35] however, the crystal structure shows that the anion symmetries are C_{2v} or lower. The assignments of the Raman spectra of $[OsO_3F][HF]_2[PnF_6]$ are based on NLDFT calculations of the $(FO_3Os\text{--}FPnF_5)_2$ dimers (see Computational Results and Table 7). Vibrational bands at frequencies higher than 1000 cm^{-1}, which are associated with the HF bridges, were not observed in the Raman spectrum.

The Raman spectra of $[OsO_3F][HF]_2[PnF_6]$ (Pn = As, Sb) are very similar, suggesting that the two compounds are

(33) Binenboym, J.; El-Gad, U.; Selig, H. *Inorg. Chem.* **1974**, *13*, 319.
(34) Gillespie, R. J.; Schrobilgen, G. J. *Inorg. Chem.* **1976**, *15*, 22.
(35) Lehmann, J. F.; Dixon, D. A.; Schrobilgen, G. J. *Inorg. Chem.* **2001**, *40*, 3002.

Table 7. Experimental and Calculated (NLDFT) Raman Frequencies and Their Assignments for $[OsO_3F][HF]_2[PnF_6]$ (Pn = As, Sb)

$[OsO_3F][HF]_2[AsF_6]$[a]			$[OsO_3F][HF]_2[SbF_6]$[b]		
freq, cm^{-1}			freq, cm^{-1}		
obsd[c]	calcd[d]	assgnt	obsd[c]	calcd[d]	assgnt
	2947(2232)	HF stretches		2868(2207)	HF stretches
	2941(223)			2863(78)	
	2455(10 326)			2381(11 674)	
	2408(3)			2334(8)	
	1223(201)	HF stretches/group rotations		1222(198)	HF bends/group rotations
	1216(87)			1218(52)	
	969(101)	Os−O stretches		968(126)	Os−O stretches + HF bends/group rotations
981(100)	969(3)		979(65)	968(22)	
971(97)	959(1)	Os−O stretches + HF bends/rotations	973(100)	965(3)	Os−O stretches + HF bends/rotations
	957(258)	Os−O stretches		963(236)	
959(26), sh	956(31)		963(25)	958(120)	Os−O stretches
	956(76)	Os−O stretches + HF bends/rotations	960(24)	957(1)	
957(33)	941(22)		954(4)	947(169)	Os−O stretches + HF bends/rotations
	938(197)		945(3)	947(6)	
	853(42)	HF bends/group rotations		862(15)	HF bends/group rotations
	846(157)			858(157)	
	768(2)			803(0)	
	759(346)			787(305)	
728(26), sh[e]	699(227)	As−F stretches		631(111)	Sb−F stretches
716(9)	697(21)		688(5)	631(1)	
	685(180)			620(182)	
710(5)	683(50)			642(161)	Os−F stretches
674(22)	666(99)		658(22)	642(2)	
	664(151)		675(8)	620(3)	Sb−F stretches
659(11)	637(54)	Os−F stretches	646(8)	608(3)	
651(9)	636(31)			607(170)	
			572(3)	566(7)	
	602(14)	As−F stretches		566(6)	
576(6)[e]	602(13)		555(2)	507(1)	Sb−F bridging + HF group stretches
491(6)	502(0)	As−F bridging + HF group stretches		506(59)	
	501(96)		501(2)	463(0)	
	464(92)			460(228)	
	463(60)			440(255)	Sb−F−Os bridging stretches
	415(172)	As−F−Os bridging stretches	391(31), sh	429(0)	
417(3)	408(9)		388(51)[e]	371(1)	
398(11), sh	385(4)			371(2)	
	384(64)			369(2)	
	374(10)		378(24)[e]	369(1)	
393(42)	372(0)		348(2)	366(0)	
	371(2)			366(1)	
371(10)	370(0)			338(89)	
364(10)	365(2)		340(2)	334(1)	
	365(8)			311(32)	
358(10)	351(4)		330(3)	311(4)	
	351(51)			290(4)	
	327(152)		311(6)	289(0)	
354(7), sh	326(6)			265(10)	
	324(95)		306(5)	264(0)	
289(10), sh[e]	323(6)		292(12)	253(0)	
282(5), sh	316(7)			250(173)	
	315(14)			247(178)	
261(3)	296(1)		281(8)	242(0)	
	295(0)			237(59)	
245(3)	274(0)		260(3)	235(0)	
	273(5)		240(6)	234(0)	
	258(26)			233(51)	
240(3)	258(4)		225(3)	228(0)	
	246(129)			228(21)	
234(6)	240(14)			209(5)	
227(6)	234(14)		218(3)	204(0)	
	230(72)			186(35)	
	223(17)		204(2)	184(0)	
221(3)	216(0)		188(1)	167(0)	
215(3)	199(0)			166(4)	
	197(67)		180(1)	156(0)	
210(3)	179(1)			152(33)	
	179(1)			146(53)	
179(2)	161(1)			136(0)	
	156(68)			131(2)	
	155(39)		145(1)	129(0)	

Table 7 (Continued)

$[OsO_3F][HF]_2[AsF_6]$[a]			$[OsO_3F][HF]_2[SbF_6]$[b]		
freq, cm^{-1}			freq, cm^{-1}		
obsd[c]	calcd[d]	assgnt	obsd[c]	calcd[d]	assgnt
167(2)	144(0)			117(1)	
	139(1)			115(0)	
144(1)	129(0)			102(5)	
	117(21)		101(2)	100(1)	
123(1)	114(0)		93(2)	81(7)	
	83(5)			80(0)	
	82(1)			66(0)	
	70(0)			64(0)	
	68(1)			62(0)	
	63(1)			62(1)	
	58(0)			48(1)	
	41(0)			43(0)	
	35(3)			37(0)	
	35(0)			35(4)	
	32(3)			32(3)	
	19(0)			29(0)	
	15(0)			22(0)	
	13(0)			19(0)	
				15(1)	
				11(0)	

[a] Spectrum recorded on the microcrystalline solid in a $^1/_4$-in. FEP sample tube at −140 °C using 647.1-nm excitation. Bands arising from the FEP sample tube were observed at 293 (14), 381 (30), 389 (30), 576 (6), 596 (1), 733 (43), and 750 (5) cm^{-1}. [b] Spectrum recorded on the solid under HF solvent in a $^1/_4$-in. FEP sample tube at −80 °C using 647.1-nm excitation. Bands arising from the FEP sample tube were observed at 292 (12), 576 (3), 596 (1), 732 (31), and 749 (3) cm^{-1}. [c] Values in parentheses denote relative Raman intensities. Abbreviation (sh) denotes a shoulder. [d] Vibrational frequencies were calculated for the optimized (NLDFT) structures of the $(FO_3Os\text{--}(HF)_2\text{--}FPnF_5)_2$ dimers. Infrared intensities in km mol^{-1} are given in parentheses. [e] This band overlaps with a band arising from the FEP sample tube.

isostructural. Three Os−O stretching modes appear 16−20 cm^{-1} lower in the Raman spectrum of $[OsO_3F][HF]_2[AsF_6]$ than those of $[OsO_3F][AsF_6]$. The band splittings are consistent with the distorted OsO_3F^+ cation found in the crystal structure of $[OsO_3F][HF]_2[AsF_6]$. A shoulder at 959 cm^{-1} and the observed splittings of the Os−O stretching bands in the Raman spectra of $[OsO_3F][HF]_2[AsF_6]$ and $[OsO_3F][HF]_2[SbF_6]$, respectively, are likely the result of vibrational coupling between two $FO_3Os\text{--}FPnF_5$ moieties which are bridged by two HF molecules in the structure of $[OsO_3F][HF]_2[AsF_6]$. The Os−O stretches of $[OsO_3F][HF][SbF_6]$ have frequencies similar to those of $[OsO_3F][HF]_2[PnF_6]$. However, all three Os−O stretches of $[OsO_3F][HF][SbF_6]$ are split by 2−5 cm^{-1}, which may be attributable to the stronger vibrational coupling that results from the shorter HF bridge in the helical structure of $[OsO_3F][HF][SbF_6]$ (see X-ray Crystallography, part d). On the basis of the calculated vibrational frequencies, comparisons with the vibrational spectra of $[NgF][PnF_6]$ (Ng = Kr, Xe; Pn = As, Sb),[34,35] and comparisons among those of the OsO_3F^+ salts, the Os−F stretches of $[OsO_3F][HF]_2[AsF_6]$, $[OsO_3F][HF]_2[SbF_6]$, and $[OsO_3F][HF][SbF_6]$ were distinguished from the Pn−F stretches and assigned to similar frequencies, namely, 652, 658, and 659 cm^{-1}, respectively. The bending modes in the Raman spectra could not be assigned because of strong vibrational coupling among these modes.

It was not possible to correlate the Os−O and Os−F stretching frequencies of the different OsO_3F^+ salts directly with their respective Os−O and Os−F bond lengths because of disorder and experimental uncertainties in the bond lengths found in the crystal structures. However, the Os−O [Os−F] stretching frequencies of $[OsO_3F][Sb_3F_{16}]$ (992−1002 [745]), $[OsO_3F][AsF_6]$ (984−996 [666]), $[OsO_3F][HF]_2[AsF_6]$ (957−981 [659]), and $[OsO_3F][HF][SbF_6]$ (960−981 [652]) decrease with increasing strength of the Os--F contacts (2.83(6), 2.66(7)/2.451(7), 2.282(5)/2.231(4), and 2.23(2)/2.240(14)/2.236(14)/2.27(2) Å, respectively), reflecting the anticipated decrease in the cationic nature of the OsO_3F moiety with increasing fluorobasicity of the anion.

(d) $[\mu\text{-}F(OsO_3F)_2][AsF_6]$. The Raman spectrum of $[\mu\text{-}F(OsO_3F)_2][AsF_6]$ exhibits six Os−O stretching bands consistent with a fluorine-bridged $\mu\text{-}F(OsO_3F)_2^+$ cation in which the two OsO_3F moieties are vibrationally coupled to each other. The splittings of the Os−O stretching bands range from 3 to 5 cm^{-1} and agree very well with the degree of coupling observed for the $\mu\text{-}F(cis\text{-}OsO_2F_3)_2^+$ cation.[1] The cation bands were assigned based on frequency calculations for the gas-phase $\mu\text{-}F(OsO_3F)_2^+$ cation at the LDFT level of theory (see Computational Results and Table 8). The number of bands associated with the AsF_6^- anion suggests a significant reduction in anion symmetry from O_h to C_{4v} or lower point symmetry. The assignments of the anion frequencies are based on those for $[XeF][AsF_6]$.[34]

The Raman band at 708 cm^{-1} is tentatively assigned to one combination of the Os−F_t (F_t: terminal fluorine) stretches and appears at lower frequency than that in $[OsO_3F][Sb_3F_{16}]$ (745 cm^{-1}), which is consistent with a lower charge density in the dinuclear cation and a correspondingly lower Os−F polarity. Similarly, the Os−O stretching frequencies of the $\mu\text{-}F(OsO_3F)_2^+$ cation are lower by 35−48 cm^{-1} than those of the OsO_3F^+ cation in $[OsO_3F][Sb_3F_{16}]$. Contacts between the cation and the AsF_6^- anion and/or HF solvent molecules are likely because the pentacoordinate osmium in $\mu\text{-}F(OsO_3F)_2^+$ is coordinately unsaturated and is supported

Table 8. Experimental and Calculated (LDFT) Raman Frequencies and Their Assignments for $[\mu\text{-}F(OsO_3F)_2][AsF_6]$

freq, cm^{-1} [a]		assgnt	
$[\mu\text{-}F(OsO_3F)_2][AsF_6]$ obsd[a]	$\mu\text{-}F(OsO_3F)_2^+$ calcd(LDFT)[b]	$\mu\text{-}F(OsO_3F)_2^+$ [c]	AsF_6^- (C_{4v})
967(100)	1001(31)	$\nu(Os'-O(1)') + \nu(Os'-O(3)')$	
963(91)	1000(85)	$\nu(Os'-O(1)') - \nu(Os'-O(3)')$	
956(45)	999(14)	$\nu(Os-O(3)) + \nu(Os-O(1))$	
953(44)	997(17)	$\nu(Os-O(3)) + \nu(Os-O(1))$	
949(29), sh	990(38)	$\nu(Os'-O(2)')$	
944(10), sh	988(41)	$\nu(Os-O(2))$	
744(2)			$\nu_8(E)$
708(8)	738(16)	$\nu(Os'-F_t') + \nu(Os-F_t)$	
	730(189)	$\nu(Os'-F_t') - \nu(Os-F_t)$	
675(6)			$\nu_1(A_1)$
651(5)			$\nu_2(A_1)$
641(5)			
603(2)			$\nu_5(B_1)$
545(1)			
493(<1)			
478(1)	476(102)	$\nu_{as}(Os--F_b--Os')$	
448(1)			$\nu_4(A_1)$
408(3), sh			
402(10)			$\nu_3(A_1)$
397(10)			$\nu_{10}(E)$
384(36)	390(0)	$\delta_s(O(2)'-Os'--F_b + O(1)-Os--F_b)$	
381(32), sh			$\nu_9(E)$
365(4)			$\nu_7(B_2)$
356(3)	336(0)	$\delta_s(O(3)-Os--F_b + O(1)'-Os'--F_b)$	
320(2)	313(1)	$\delta(O(1)'-Os'-O(3)')$	
	312(2)	$\delta(O(1)-Os-O(2)) + \delta(O(1)'-Os'-O(2)')$	
	308(1)	$\delta(O(2)-Os-O(3)) + \delta(O(2)'-Os'-O(3)')$	
	298(0)	$\delta(O(3)-Os-F_t) + \delta(O(3)'-Os'-F_t') +$ other $\delta(O-Os-F)$	
	296(1)	$\delta(O(3)-Os-F_t) - \delta(O(3)'-Os'-F_t') +$ other $\delta(O-Os-F)$	
	292(1)	$\delta(O(2)-Os-F_t) - \delta(O(2)'-Os'-F_t')$	
	280(1)	$\delta_{o.pl.}(OsO_3) - \delta_{o.pl.}(Os'-O'_3)$	
250(2)	269(7)	$\delta(F_t-Os--F_b) + \delta(F_t'-Os--F_b)$	
240(4)			
235(4)	213(15)	$\delta_s(F_t-Os--F_b)$	
182(2)	192(169)	$\delta_{o.pl.}(OsO_3) + \delta_{o.pl.}(Os'O'_3)$	
176(1)			
167(1)			
159(1)			
152(1)	147(0)	antisym rocking of OsO_3F groups toward F_b	
139(2)	132(15)	sym rocking of OsO_3F groups toward F_b	
117(1)	127(5)	$\nu_s(Os--F_b--Os')$	
81(2)	88(0)	$\delta_{i.p.}(Os--F_b--Os')$	
	54(1)	$\delta_{o.o.p.}(Os--F_b--Os')$	
	43(0)	antisym torsion of OsO_3F groups around F_b	

[a] Spectrum recorded on the solid under liquid HF solvent in a 1/4-in. FEP sample tube at −80 °C using 647.1-nm excitation. Values in parentheses denote relative Raman intensities. Abbreviation (sh) denotes a shoulder. Bands arising from the FEP sample tube were observed at 292 (8), 576 (2), 732 (18), and 751 (2) cm^{-1}. [b] Infrared intensities in km mol^{-1} are given in parentheses. [c] The abbreviations i.p. and o.o.p. denote in-plane and out-of-plane bends, respectively.

by the significant lowering of the anion symmetry and the instability of the cation in the absence of HF solvent (vide supra). Consequently, assignments of the bending modes based on the calculated frequencies for the gas-phase cation must be viewed as tentative.

Computational Results. Previous work in our laboratories has shown that electronic structure calculations, usually at the density functional theory (DFT) level, are a valuable tool for understanding the structures and vibrational frequencies of transition metal oxide fluorides.[1,4,36] For the Os complexes, we benchmarked the method by calculating the geometry and vibrational frequencies of OsO_4 (Table 9) for which there are well-established experimental values for the free molecules.[37,38] The calculated bond distance for OsO_4 is in very good agreement with the experimental value. The calculated harmonic stretching frequencies are higher than the experimental anharmonic frequencies by 22 and 29 cm^{-1}. The calculated frequencies of the bending modes are 4 and 6 cm^{-1} lower than the experimental frequencies. This behavior is typical of that found at the local DFT (LDFT) level; i.e., the calculated stretching frequencies are too high and the bending frequencies are too low.[4]

(a) OsO_3F^+. The fully optimized geometry of OsO_3F^+ cation possesses C_{3v} symmetry. The weighted average of the calculated Os−O and Os−F bond lengths (1.721 Å, Table 9) is within 3σ of the average experimental bond length of 1.68(3) Å for the Os−O and Os−F bonds in the disordered $[OsO_3F][Sb_3F_{16}]$ structure. The calculated Os−O and Os−F bond lengths in the OsO_3F^+ cation are shorter than the

(36) Christe, K. O.; Dixon, D. A.; Mack, H. G.; Oberhammer, H.; Pagelot, A.; Sanders, J. C. P.; Schrobilgen, G. J. *J. Am. Chem. Soc.* **1993**, *115*, 11279.

(37) Krebs, B.; Hasse, K.-D. *Acta Crystallogr., Sect. B* **1976**, *32*, 1334.
(38) Huston, J. L.; Claassen, H. H. *J. Chem. Phys.* **1970**, *52*, 5646.

Table 9. Calculated Geometries for OsO_4, OsO_3F^+,[a] ReO_3F,[a] $F(OsO_3F)_2^+$, and the $(FO_3Os\text{--}(HF)_2\text{--}FSbF_5)_2$ Dimer and Vibrational Frequencies for OsO_4

OsO_4			OsO_3F^+		ReO_3F		
	calcd(LDFT)	expt[b]		calcd(LDFT)		calcd(LDFT)	expt[c]
Os−O	1.717 Å	1.698 Å	Os−O	1.690 Å	Re−O	1.703 Å	1.692(3) Å
		1.727 Å	Os−F	1.812 Å	Re−F	1.843 Å	1.859(8) Å
			O−Os−F	110.9°	O−Re−F	110.6°	109.5(3)°
			F−Os−F	108.0°			
	freq, cm^{-1}						
$\nu_1(A)$	994(0)	965.2					
$\nu_2(E)$	329(0)	333.1					
$\nu_3(T_2)$	982(316)	960.1					
$\nu_4(T_2)$	317(10)	322.7					

$[FO_3Os\text{--}F_b\text{--}OsO_3F]^+$, calcd(LDFT)

Os−O(1)/Os′−O(1)′	1.702/1.702 Å	O(1)−Os−O(2)/O(1)′−Os′−O(2)′	117.5/117.4°	O(1)−Os--F_b--Os/Os--F_b--Os−O(1)	137.3/137.3°
Os−O(2)/Os′−O(2)′	1.708/1.707 Å	O(1)−Os−O(3)/O(1)′−Os′−O(3)′	117.2/116.8°	O(2)−Os--F_b--Os/Os--F_b--Os−O(2)	17.0/16.7°
Os−O(3)/Os′−O(3)′	1.704/1.703 Å	O(2)−Os−O(3)/O(2)′−Os′−O(3)′	116.9/116.7°	O(3)−Os--F_b--Os/Os--F_b--Os−O(3)	−102.4/−102.6°
Os--F_b/Os--F_b	2.129/2.140 Å	O(1)−Os--F_b/O(1)′−Os′--F_b	79.3/78.8°	F_t−Os--F_b--Os/Os--F_b--Os−F_t	165.8/151.4°
Os−F_t/Os′−F_t′	1.824/1.823 Å	O(2)−Os--F_b/O(2)′−Os′--F_b	81.1/80.6°		
		O(3)−Os--F_b/O(3)′−Os′--F_b	80.4/80.2°		
		O(1)−Os−F_t/O(1)′−Os′−F_t′	99.5/99.8°		
		O(2)−Os−F_t/O(2)′−Os′−F_t′	100.1/100.4°		
		O(3)−Os−F_t/O(3)′−Os′−F_t′	99.7/100.2°		
		F_b--Os−F_t/F_b--Os′−F_t′	178.1/178.5°		
		Os--F_b--Os′	138.4°		

$(FO_3Os\text{--}(HF)_2\text{--}FSbF_5)_2$[d]

	LDFT	NLDFT		LDFT	NLDFT		LDFT	NLDFT
Os−O(1)	1.703/1.703	1.719/1.719	O(1)−Os−O(2)	103.9/103.9	103.3/103.3	O(1)−Os−O(3)	103.7103.7	103.3/103.3
Os−O(2)	1.702/1.702	1.715/1.715	O(2)−Os−O(3)	103.2/103.2	104.1/104.1	O(1)−Os−F(1)	98.2/97.8	97.5/97.5
Os−O(3)	1.708/1.708	1.721/1.720	O(2)−Os−F(1)	96.9/96.9	99.8/99.8	O(3)−Os−F(1)	145.6/145.8	143.5/143.5
Os−F(1)	1.871/1.872	1.891/1.890	O(2)−Os--F(3)	86.1/86.1	87.9/87.8	O(1)−Os--F(3)	168.0/167.9	166.6/166.6
Os--F(2)	2.155/2.156	2.320/2.320	O(3)−Os--F(3)	80.1/80.2	80.7/80.7	F(1)−Os--F(3)	73.6/73.8	72.9/73.0
Os--F(3)	2.226/2.221	2.264/2.265	O(2)−Os--F(2)	163.7/163.6	167.8/167.8	O(1)−Os--F(2)	90.2/90.3	86.7/86.8
Sb−F(3)	2.033/2.034	2.089/2.089	O(3)−Os--F(2)	80.8/80.8	79.9/79.9	F(1)−Os--F(2)	72.7/72.8	71.6/71.6
Sb−F(4)	2.017/2.017	2.026/2.026	F(3)--Os--F(2)	79.0/78.9	81.3/81.4	As−F(3)--Os	125.1/124.6	132.4/132.0
Sb−F(5)	1.914/1.914	1.945/1.945	F(3)−As−F(4)	82.4/82.2	84.6/84.7	F(3)−As−F(5)	85.0/85.0	84.1/84.2
Sb−F(6)	1.907/1.908	1.940/1.940	F(3)−As−F(6)	88.5/88.3	86.8/86.7	F(3)−As−F(7)	84.5/84.3	85.5/85.5
Sb−F(7)	1.908/1.908	1.939/1.939	F(3)−As−F(8)	172.2/172.3	175.7/175.8	F(4)−As−F(5)	85.3/85.2	86.7/86.7
Sb−F(8)	1.905/1.905	1.935/1.935	F(4)−As−F(6)	170.8/170.6	171.3/171.3	F(4)−As−F(7)	84.3/84.5	85.5/85.4
F(2)−H(1)	1.103/1.103	1.031/1.031	F(4)−As−F(8)	89.9/90.0	91.3/91.2	F(5)−As−F(6)	93.4/93.2	92.6/92.7
H(1)--F(9)	1.192/1.193	1.353/1.352	F(5)−As−F(7)	166.1/166.1	167.6/167.5	F(5)−As−F(8)	94.5/94.7	94.6/94.6
F(9)−H(2)	1.056/1.056	1.005/1.005	F(6)−As−F(7)	95.4/95.4	93.6/93.6	F(6)−As−F(8)	99.3/99.4	97.4/97.4
H(2)--F(4A)	1.270/1.272	1.430/1.431	F(7)−As−F(8)	94.7/94.6	95.3/95.2	F(9)−H(2)--F(4A)	176.7/176.5	175.7/175.8
F(2)···F(9)		2.382/2.383	H(2)−F(9)--H(1)	115.2/115.2	117.1/117.2	F(2)−H(1)--F(9)	178.3/178.3	178.7/178.7
F(9)···F(4A)		2.434/2.434	Os--F(2)−H(1)	122.9/122.9	122.0/122.1	As−F(4)--H(2A)	122.9/122.7	127.4/127.6

[a] The vibrational frequencies for OsO_3F^+ and ReO_3F are given in Table 2. [b] Bond lengths for crystalline OsO_4 are from ref 37; Raman frequencies for gaseous OsO_4 are from ref 38. [c] Bond lengths for ReO_3F are from a microwave study.[10] [d] The atom numbering scheme used for $(FO_3Os\text{--}(HF)_2\text{--}FSbF_5)_2$ is the same as that used in the crystal structure of $[OsO_3F][HF]_2[AsF_6]$; the two calculated values for each distance and angle refer to the two distances and angles that are found to be symmetry related in the crystal structure of $[OsO_3F][HF]_2[AsF_6]$.

calculated bond lengths in monomeric OsO_3F_2 [4] by 0.027 and 0.077 Å, respectively, consistent with cation formation. The calculated geometrical parameters for ReO_3F (Table 9), which is isoelectronic with the OsO_3F^+ cation, are in good agreement with the experimental data, with the calculated Re−F and Re−O bond distances being too short by 0.016 and 0.011 Å, respectively. This suggests that the bond distances calculated for isolated OsO_3F^+ should be within 0.02 Å of the experimental values. Consistent with the positive charge on OsO_3F^+, the Os−O and Os−F bond distances are shorter than the respective Re−O and Re−F bond lengths of neutral isoelectronic ReO_3F.

The stretching frequencies for OsO_3F^+ (ReO_3F) (Table 4), calculated at the LDFT level, are higher by 10−36 (11−16) cm^{-1} than the experimental values, whereas the calculated bending modes are lower by 14−18 (13−24.5) cm^{-1}. This systematic error at the LDFT level has been noted above. The slightly larger deviation between the calculated and experimental values in the Os−O stretches compared with the Re−O stretching frequencies can be partially accounted for by cation−anion contacts in the solid state, which would lower the experimental values with respect to those calculated for the gas-phase ion.

(b) μ-$F(OsO_3F)_2^+$. The fully optimized gas-phase geometry of the μ-$F(OsO_3F)_2^+$ cation calculated at the local (LDFT) level of theory contains two slightly asymmetric fluorine bridges with Os--F_b (2.129 Å) being slightly shorter than Os′--F_b (2.140 Å). The calculated structure for the dinuclear cation has a trigonal bipyramidal environment about each osmium with the oxygens in the equatorial plane and the terminal (F_t) and bridging fluorines (F_b) in the axial positions (Table 9). The three equatorial oxygens are bent

toward the weak axial Os--F_b bond with O−Os−F_t bond angles close to 100°. The calculated Os−O and Os−F_t bond lengths are intermediate with respect to those calculated for monomeric OsO_3F_2[4] and the OsO_3F^+ cation. The calculated Os−O and Os−F stretching frequencies for the μ-$F(OsO_3F)_2^+$ cation (Table 8) agree well with the experimental values considering the systematic error, with the experimental stretching frequencies being 34−44 cm^{-1} higher than the observed values. The large discrepancy between the calculated and experimental frequencies can also be attributed to the expected contacts between the cation and the AsF_6^- anion (see Raman Spectroscopy, part d). The antisymmetic Os--F_b--Os′ stretching frequency was calculated to be 476 cm^{-1}. The unambiguous assignment of an experimental frequency to the bridging stretch is not possible because of the large number of weak Raman bands in this region.

(c) $(FO_3Os\text{--}FPnF_5)_2$ and $(FO_3Os\text{--}(HF)_2\text{--}FPnF_5)_2$. The gas-phase geometries of the $(FO_3Os\text{--}FPnF_5)_2$ and $(FO_3Os\text{--}(HF)_2\text{--}FPnF_5)_2$ dimers were calculated at the LDFT and NLDFT level of theory, and their experimental centrosymmetric symmetries were reproduced by the calculations with good accuracy for the $(FO_3Os\text{--}FAsF_5)_2$ dimer and with fair agreement for the $(FO_3Os\text{--}(HF)_2\text{--}FAsF_5)_2$ dimer (Table 2). The calculated $(FO_3Os\text{--}FAsF_5)_2$ dimer at the local DFT level comprises two equivalent contacts between each osmium and two bridging fluorines of 2.289 Å, contrasting with the experimental structure, which contains two significantly different bridges, i.e., Os(1)--F(4) (2.451(7) Å) and Os(1)--F(2) (2.666(7) Å). The Os--F fluorine bridge bonds are shorter by 0.377 and 0.162 Å in the LDFT calculations, respectively. The calculations at the nonlocal level reproduce the asymmetry of the F bridges in the experimental structure of the $(FO_3Os\text{--}FAsF_5)_2$ dimer with Os--F distances of 2.417 and 2.293 Å. The large interactions between the cations and anions at the LDFT and NLDFT levels are consistent with other work[35] which shows that LDFT and NLDFT exaggerate intermolecular interactions leading to interactions that are too strong. While the calculated Os−O bond lengths in the $(FO_3Os\text{--}FPnF_5)_2$ dimers are the same as the experimental values at the LDFT level, the calculated Os−O (NLDFT), Os(1)−F(1) (LDFT and NLDFT), and terminal Pn−F (LDFT and NLDFT) bond lengths are significantly longer than the experimental values. In general, the bond lengths at the nonlocal level are significantly longer than those calculated at the local level.

The dimer structures with two HF molecules bridging an OsO_3F/PnF_6 cation/anion pair are difficult to describe, both experimentally and computationally. Experimentally, it is difficult to observe the hydrogen atoms by X-ray diffraction and we have found it difficult to predict the structures of isolated ion pairs with methods that are computationally fast enough to deal with such large species.[35] As noted above, the computation tends to make the ion pair too strongly bound. This arises because the pair is not embedded in a crystalline environment so that each ion only sees the adjacent charged species and is more strongly attracted to it. Examination of the structures calculated at the local and nonlocal levels for the dimers without $(HF)_2$ showed that the nonlocal calculation better reproduced the experimental results, giving larger differences between the Os(1)−F(2) and Os(1)−F(4) bonds, which are consistent with the experimental values. Examination of the structures of the HF-bridged dimers at the nonlocal level shows that the H−F bonds are elongated with respect to that of free HF (0.94 Å) by 0.06 and 0.09 Å. The two H−F bonds of 1.00 and 1.03 Å are significantly shorter than the H−F bonds of 1.14 Å in HF_2^- [39] while the other H--F interactions are much longer (1.46 and 1.36 Å). Clearly, these species are closer to HF molecules than to an HF_2^- anion in their structures. The geometry at the local level is closer to the bifluoride anion than to the HF molecule. The F···F distances between the HF molecules in the Os/As and Os/Sb dimers are 2.298 and 2.382 Å, respectively, compared with the experimental values of 2.429(8) Å for the $(FO_3Os\text{--}(HF)_2\text{--}FAsF_5)_2$ dimer and are clearly similar to the F···F distance of 2.278 Å in the HF_2^- anion.[39] At the nonlocal level, the Os−F(H) bond distance is quite long with 2.34 Å for the Os/As dimer and 2.32 Å for the Os/Sb dimer, in reasonable agreement with the experimental value of 2.282(5) Å for the Os/As dimer. As expected, these distances are much shorter at the local level with 2.16 Å for both dimers. This is consistent with the higher predicted ionicity of the $(HF)_2$ bridged species at the local level, which is closer to an $[FHF]^-$ anion, and should lead to shorter and stronger H--F hydrogen bonding interactions as calculated.

The HF molecules are, however, clearly elongated in the dimer. The calculated frequency of the HF molecule at the nonlocal level is 3984 cm^{-1} and at the local level it is 4009 cm^{-1} compared with an experimental harmonic value of 4139 cm^{-1}.[40] The calculated frequencies at the nonlocal level for the two shorter bonds are close to 2950 cm^{-1} and are in the range 2400−2450 cm^{-1} for the two longer HF bonds. The local values are significantly lower, at ca. 2500 cm^{-1} and 1800−1900 cm^{-1}, respectively. The calculated values for the $[FHF]^-$ anion at the local (nonlocal) level are 1912 (1668) cm^{-1} for the asymmetric stretch $\nu_3(\Sigma_u^+)$, 1277 (1296) cm^{-1} for the bend $\nu_2(\Pi_u)$, and 620 (602) cm^{-1} for the symmetric stretch $\nu_1(\Sigma_g^+)$. The experimental frequencies for $[HF_2]^-$ in its $[N(CH_3)_4]^+$ salt are 596 cm^{-1} ($\nu_1(\Sigma_g^+)$),[17] 1264−1255 cm^{-1} ($\nu_2(\Pi_u)$),[41] and 1376 cm^{-1} ($\nu_3(\Sigma_u^+)$).[41] As noted above, the H−F bond strength of the nonlocal dimer structure is closer to that of a free HF molecule than to that of the $[FHF]^-$ anion, although the calculated frequencies are significantly lower than those in free HF because the F−H bonds in the dimer are calculated to be elongated by less than 0.1 Å. However, for the structure at the local level, the lower frequency stretches for the HF molecules are in the predicted range for the asymmetric stretch of the $[FHF]^-$ anion. The calculated infrared spectra contain intense bands in the HF stretching region. These correspond to asymmetric HF stretches with extended HF bonds in an extremely polar

(39) Kawaguchi, K.; Hirota, E. *J. Chem. Phys.* **1987**, *87*, 6838.
(40) Nakamoto, K. *Infrared and Raman Spectra of Inorganic and Coordination Compound, Part A*, 5th ed.; John Wiley and Sons: New York, 1997; p.154.
(41) Harmon, K. M.; Lovelace, R. R. *J. Phys. Chem.* **1982**, *86*, 900.

Table 10. Mulliken Charges, Mayer Valencies, and Mayer Bond Orders for OsO_4, OsO_3F^+, ReO_3F, and μ-$F(OsO_3F)_2^+$

Mulliken Charges

OsO_4		OsO_3F^+		ReO_3F		μ-$F(OsO_3F)_2^+$	
Os	1.77	Os	1.93	Re	1.73	Os/Os′	1.86/1.86
O	−0.44	O	−0.23	O	−0.45	O(1)/O(1)′	−0.28/−0.27
		F	−0.24	F	−0.39	O(2)/O(2)′	−0.34/−0.34
						O(3)/O(3)′	−0.28/−0.28
						F_b	−0.43
						F_t/F_t'	−0.25/−0.25

Mayer Valencies

OsO_4		OsO_3F^+		ReO_3F		μ-$F(OsO_3F)_2^+$	
Os	5.96	Os	5.77	Re	5.85	Os/Os′	5.98/5.99
O	2.25	O	2.42	O	2.25	O(1)/O(1)′	2.36/2.36
		F	1.22	F	1.00	O(2)/O(2)′	2.29/2.29
						O(3)/O(3)′	2.36/2.36
						F_b	0.69
						F_t/F_t'	1.20/1.20

Mayer Bond Orders

OsO_4		OsO_3F^+		ReO_3F		μ-$F(OsO_3F)_2^+$	
Os−O	1.49	Os−O	1.65	Re−O	1.70	Os−O(1)	1.64
		Os−F	0.81	Re−F	0.74	Os−O(2)	1.58
						Os−O(3)	1.64
						Os--F_b	0.32
						Os−F_t	0.81

regime. This leads to a very large predicted infrared absorption of the order of 10^4 km mol^{-1} in the 2000−3000 cm^{-1} region. Unfortunately, it was not possible to obtain experimental infrared spectra of $[OsO_3F][HF]_2[PnF_6]$ (Pn = As and Sb), because the two compounds readily lose HF upon isolation of the solids from HF solution.

The DFT calculations predict the interactions of the isolated cations and anions to be too large when compared with interactions in the solid state. As expected, local DFT calculations which generally lead to overbinding for weak interactions, lead to the largest errors. We have thus used the nonlocal results in the discussion of the vibrational frequencies, which are given in Tables 5 and 7 for $[OsO_3F][PnF_6]$ and $[OsO_3F][HF]_2[PnF_6]$, respectively. There are some generalities that are found. The Os−O stretches are all predicted to be in the region of 955−975 cm^{-1} except for the HF-bridged dimers where HF bends can mix and lower the Os−O stretches to as low as 938 cm^{-1}. The Os−F stretches are all predicted to be near 650 ± 10 cm^{-1} with the HF dimers at the lower end. For the dimers not containing bridging HF molecules, the stretches involving the bridging F atoms are predicted to occur in two pairs with one pair near 500 cm^{-1} and the second pair in the region 430−460 cm^{-1}. In the dimers containing bridging HF molecules, the Os--F−Pn stretches occur as pairs in similar regions, i.e., 430−440 cm^{-1} for the Sb dimer and at ca. 410 cm^{-1} for the As dimer. The stretches of the As−F fluorines involved with the HF molecules are in the range 460−500 cm^{-1}, and mixing occurs with the HF group stretches and the motion of the HF molecule moving between the Os and Pn atoms. For comparison, the OsO_3F^+ frequencies at the nonlocal level are given in Table 4. The Os−O and Os−F stretches in the dimers are shifted to lower frequencies by 30 and 50−70 cm^{-1}, respectively, compared with the gas-phase OsO_3F^+ cation. The sequence for the calculated Os−F and the high-frequency Sb−F stretching modes appears to be wrong on the basis of the assumption that the Os−F stretching frequencies of the two $(FO_3Os\text{--}(HF)_2\text{--}FPnF_5)_2$ dimers do not differ by more than 5 cm^{-1}, as predicted by the NLDFT calculations. This is a consequence of the underestimated terminal Sb−F bond strength. The low-frequency bending and torsional modes of the dimers are strongly coupled and are not assigned and discussed further.

(d) Charges, Valencies, and Bond Orders. The calculated Mulliken charges, Mayer valencies, and Mayer bond orders for OsO_4, OsO_3F^+, ReO_3F, and μ-$F(OsO_3F)_2^+$ are given in Table 10. The calculated values for the $(FO_3Os\text{--}FAsF_5)_2$ and $(FO_3Os\text{--}(HF)_2\text{--}FAsF_5)_2$ dimers are given in Table 11 (Supporting Information) and will not be discussed. Abstraction of a fluoride ion from OsO_3F_2 leads to an increase in the positive charge of osmium from 1.76[4] to 1.93 and a decrease in the Mayer valency of osmium from 6.31[4] to 5.77. The negative charges on the oxygens and fluorines and their valencies decrease when compared with those of OsO_3F_2. Whereas the Os−O bond order increases only slightly upon fluoride ion abstraction (from 1.63[4] to 1.65), the Os−F bond becomes significantly less polar. The calculated charges and valencies for osmium and oxygen and the Os−O bond orders for the dinuclear $[FO_3Os\text{--}F_b\text{--}OsO_3F]^+$ cation lie between those found for the OsO_3F^+ cation and monomeric OsO_3F_2.[4] The Os−F_t bond order is the same in the dinuclear cation as in OsO_3F^+, and the charges and valencies for the terminal fluorines in both cations differ only slightly. The Os--F_b bond order (0.32) is less than half of that for the terminal fluorines (0.81), and the negative charge (−0.43) [valency (0.69)] on the bridging fluorine is significantly higher [lower] than the negative charge (−0.25) [valency (1.20)] for the terminal fluorine. This reflects the high degree of ionicity of the fluorine bridge bonds and agrees with the dissociation observed in the

experiment (see Syntheses of the OsO_3F^+ and μ-$F(OsO_3F)_2^+$ Cations and Solution Characterization of the OsO_3F^+ Cation by ^{19}F NMR Spectroscopy), which is facilitated by the formation of contacts with anions and donor solvent molecules.

Conclusion

Osmium trioxide difluoride behaves as a fluoride ion donor toward the strong Lewis acids AsF_5 and SbF_5 in HF solvent. The OsO_3F^+ cation is highly electrophilic and expands its coordination sphere in the solid state by the formation of contacts with the AsF_6^- and SbF_6^- anions and HF molecules. The X-ray crystal structures of $[OsO_3F][HF]_2[AsF_6]$ and $[OsO_3F][HF][SbF_6]$ contain HF bridged cyclic $(FO_3Os\text{--}(HF)_2\text{--}FAsF_5)_2$ dimers and helical $(FO_3Os\text{--}FH\text{--}FSbF_5)_\infty$ chains, respectively, that provide new and rare examples of HF coordinated to metal centers. The resulting hexacoordination about osmium has a *fac*-trioxo arrangement. The weakly nucleophilic $Sb_3F_{16}^-$ anion and the absence of a donor solvent such as HF are necessary to stabilize an OsO_3F^+ cation having only weak contacts to the counteranion and tetrahedral coordination. The dinuclear μ-$F(OsO_3F)_2^+$ cation was observed by Raman spectroscopy with AsF_6^- as the counteranion and was shown to readily dissociate, which is consistent with the weak bridging Os--F bond length calculated by LDFT methods.

Experimental Section

Apparatus and Materials. Volatile materials were handled on vacuum lines constructed of nickel, stainless steel, FEP, and Pyrex, and nonvolatile materials were handled in the atmosphere of a drybox as previously described.[42]

The starting compounds, OsO_3F_2,[5] AsF_5,[43] SbF_5,[44] and SbF_3,[41] were prepared by standard literature methods. Sulfuryl chloride fluoride, SO_2ClF (Aldrich), was purified by the standard literature methods[45] and stored over anhydrous KF. Anhydrous HF (Harshaw Chemical Co.) was dried and purified by the standard literature methods.[46]

Synthesis of $[OsO_3F][HF]_2[AsF_6]$, $[\mu$-$F(OsO_3F)_2][AsF_6]$, and $[OsO_3F][AsF_6]$ and Crystal Growth of $[OsO_3F][AsF_6]$. Inside a drybox, 0.09203 g (0.333 mmol) of OsO_3F_2 was loaded into a $^1/_4$-in. o.d. FEP reaction tube equipped with a Kel-F valve. Approximately 0.5 mL of HF was condensed into the tube at −196 °C followed by condensation of ca. 0.7 mmol of AsF_5. Osmium trioxide difluoride dissolved upon warming to ambient temperature yielding a clear yellow-orange solution. The bulk of the HF solvent and excess AsF_5 were removed by pumping at −78 °C for ca. 3 h and resulted in the formation of an orange, crystalline precipitate under ca. 0.1 mL of HF, which was identified by Raman spectroscopy as $[OsO_3F][HF]_2[AsF_6]$. Addition of ca. 0.5 mmol of AsF_5 and 0.57 mL of HF followed by complete removal of the HF solvent at −78 °C over a period of ca. 5 h yielded straw-yellow $[OsO_3F][AsF_6]$. Distillation of ca. 0.3 mL of HF onto the solid resulted in a yellow solution above a heterogeneous mixture of yellow ($[OsO_3F][AsF_6]$) and orange ($[\mu$-$F(OsO_3F)_2][AsF_6]$) solids at −78 °C, which was confirmed by Raman spectroscopy. Thorough agitation at −78 °C resulted in an orange precipitate comprised exclusively of $[\mu$-$F(OsO_3F)_2][AsF_6]$, which presumably arises because $[OsO_3F][AsF_6]$ has a significantly higher solubility than $[\mu$-$F(OsO_3F)_2][AsF_6]$. Condensation of an additional 0.4 mmol of AsF_5 onto the mixture resulted in complete dissolution of the solid close to room temperature and did not yield a precipitate at −78 °C. Approximately 0.05 mL of HF was removed at −78 °C resulting in a yellow precipitate which was identified by Raman spectroscopy as $[OsO_3F][AsF_6]$. After redissolving the precipitate in the HF/AsF_5 mixture at approximately room temperature, the sample was cooled to −78 °C and yellow crystals grew over a 12 h period. The solvent was removed under dynamic vacuum at −78 °C, and yellow crystals were selected and mounted at −110 °C as previously described.[4] The crystal used in this study had the dimensions 0.12 × 0.10 × 0.10 mm^3.

An NMR sample in a 4-mm. o.d. FEP tube was prepared using 0.0303 g (0.1097 mmol) of OsO_3F_2, 0.2 mL of HF, and 1.5 mmol of AsF_5 (ca. 13.5-fold molar excess).

Crystal Growth of $[OsO_3F][HF]_2[AsF_6]$. Crystals of $[OsO_3F][HF]_2[AsF_6]$ were obtained from a sample composed of 0.1032 g (0.374 mmol) of OsO_3F_2 and ca. 0.9 mmol of AsF_5 in 0.85 mL of HF. Orange crystals of $[OsO_3F][HF]_2[AsF_6]$ were grown by slow removal of the HF solvent and excess AsF_5 under dynamic vacuum at −78 °C. After almost complete removal of the HF solvent, a portion of the crystalline sample turned yellow ($[OsO_3F][AsF_6]$). Pumping was discontinued, and the FEP tube was immediately back-filled with dry nitrogen while maintaining the sample at −78 °C. Orange crystals were selected and mounted at −117 °C as previously described.[4] The crystal used in this study had the dimensions 0.25 × 0.20 × 0.05 mm^3.

Syntheses of $[OsO_3F][HF][SbF_6]$ and $[OsO_3F][HF]_2[SbF_6]$ and Crystal Growth of $[OsO_3F][HF][SbF_6]$. Inside the drybox, 0.03962 g (0.2217 mmol) of SbF_3 was transferred into the vertical arm of a $^1/_4$-in. o.d. FEP T-shaped reactor equipped with a Kel-F valve. After condensation of approximately 0.6 mL of HF onto the SbF_3, the mixture was allowed to react with F_2 at room temperature until white solid SbF_3 had completely reacted to form SbF_5 and had dissolved. Inside the drybox, 0.06342 g (0.2296 mmol) of OsO_3F_2 was added to the frozen solution. Warming to room temperature yielded a clear, yellow-orange solution. Upon cooling to −78 °C, clusters of orange needles grew and were identified as $[OsO_3F][HF]_2[SbF_6]$ by Raman spectroscopy. Removal of the HF solvent at −78 °C and brief pumping at room temperature yielded solid straw-yellow $[OsO_3F][HF][SbF_6]$. After redissolution of $[OsO_3F][HF][SbF_6]$ in approximately 0.6 mL of HF at room temperature and cooling to −78 °C, orange, crystalline clusters and yellow plates grew over a period of ca. 12 h. The HF supernatant was decanted into the sidearm of the T-reactor, which was subsequently heat sealed off at −196 °C under dynamic vacuum while the crystals were dried at −75 °C under dynamic vacuum. Yellow plates were selected and mounted at −100 °C as previously described.[4] The crystal used in this study had the dimensions 0.08 × 0.04 × 0.03 mm^3.

In a separate experiment using 0.0538 g (0.3010 mmol) of SbF_3, 0.0695 g (0.2516 mmol) of OsO_3F_2 and ca. 0.6 mL of HF, small amounts of $[OsO_3F][SbF_6]$ were observed by Raman spectroscopy upon removal of the HF solvent (pumped on for 3 h at −78 °C and for 5 min at room temperature). Pumping at room temperature for 5 h did not increase the amount of $[OsO_3F][SbF_6]$ significantly.

(42) Casteel, W. J., Jr.; Kolb, P.; LeBlond, N.; Mercier, H. P. A.; Schrobilgen, G. J. *Inorg. Chem.* **1996**, *35*, 929.
(43) Mercier, H. P. A.; Sanders, J. C. P.; Schrobilgen, G. J.; Tsai, S. S. *Inorg. Chem.* **1993**, *32*, 386.
(44) LeBlond, N.; Dixon, D. A.; Schrobilgen, G. J. *Inorg. Chem.* **2000**, *39*, 2473.
(45) Schrobilgen, G. J.; Holloway, J. H.; Granger, P.; Brevard, C. *Inorg. Chem.* **1978**, *17*, 980.
(46) Emara, A. A. A.; Schrobilgen, G. J. *Inorg. Chem.* **1992**, *31*, 1323.

The sample liquified at 45 °C and was pumped on at this temperature for a further 2 h using a mercury diffusion pump, resulting in a decrease in the relative Raman intensities of the OsO_2 stretches of $[OsO_3F][SbF_6]$ when compared with those of $[OsO_3F][HF][SbF_6]$. Distillation of 0.6 mL of HF onto the solid resulted in dissolution of the solid at room temperature and slow precipitation of yellow $[OsO_3F][HF][SbF_6]$. Reduction of the solution volume to 0.17 mL at −78 °C followed by redissolution of the solid at room-temperature resulted in the precipitation of $[OsO_3F][HF]_2[SbF_6]$ at −78 °C.

Synthesis and Crystal Growth of $[OsO_3F][Sb_3F_{16}]$. Inside a dry nitrogen filled glovebag, 0.9393 g (4.334 mmol) of SbF_5 was syringed into a $^1/_4$-in. o.d. FEP reaction tube equipped with a Kel-F valve, and 0.0847 g (0.3067 mmol) of OsO_3F_2 was added to the frozen SbF_5 sample inside a drybox (ca. −140 °C). The reaction mixture was warmed to 55 °C outside the drybox, yielding a clear straw-yellow solution upon sonication. The solution was placed in a water bath at 55 °C and allowed to cool to 35 °C for 2 h yielding copious amounts of thin straw-yellow plates. Excess SbF_5 was removed under dynamic vacuum at ambient temperature over a period of 5.5 h yielding 0.2906 g of straw-yellow plates of $[OsO_3F][Sb_3F_{16}]$ (theoretical, 0.2841 g) corresponding to a molar ratio of SbF_5:OsO_3F_2 = 3.1:1.0. Crystals were selected and mounted at −120 °C as previously described.[4] The crystal used in this study had the dimensions 0.14 × 0.10 × 0.005 mm^3.

A ^{19}F NMR sample of OsO_3F_2, dissolved in neat SbF_5, was prepared in a $^1/_4$-in. o.d. FEP tube equipped with a Kel-F valve using 0.0538 g (0.1948 mmol) of OsO_3F_2 and 2.41 g (11.1 mmol) of SbF_5. Samples for ^{19}F NMR spectroscopy were also prepared in 4-mm o.d. FEP tubes equipped with Kel-F valves by dissolving 0.0274 g (0.0296 mmol) [0.0302 g (0.0326 mmol)] of $[OsO_3F][Sb_3F_{16}]$ in ca. 0.35 mL of SO_2ClF [0.18 mL of HF], yielding a clear yellow solution upon warming to −78 °C. Sample tubes were heat sealed under dynamic vacuum at −196 °C.

X-ray Structure Determinations. (a) Collection and Reduction of X-ray Data. X-ray diffraction data were collected using a P4 Siemens diffractometer equipped with a Siemens SMART 1K charge-coupled device (CCD) area detector (using the program SMART)[47] and a rotating anode using graphite-monochromated Mo Kα radiation (λ = 0.710 73 Å). The crystal-to-detector distances for $[OsO_3F][AsF_6]$, $[OsO_3F][SbF_6]$, $[OsO_3F][HF]_2[AsF_6]$, $[OsO_3F][HF][SbF_6]$, and $[OsO_3F][Sb_3F_{16}]$ were 4.9870, 4.9870, 5.000, 4.9870, and 5.0140 cm, respectively, and the data collections were carried out in 512 × 512 pixel mode using 2 × 2 pixel binning. Complete spheres of data were collected to better than 0.8 Å resolution. Processing was carried out by using the program SAINT,[47] which applied Lorentz and polarization corrections to three-dimensionally integrated diffraction spots. The program SADABS[48] was used for the scaling of diffraction data, the application of a decay correction, and an empirical absorption correction based on redundant reflections.

(b) Solution and Refinement of the Structures. All calculations were performed using the SHELXTL Plus package[49] for structure determination, refinement, and molecular graphics.

The XPREP program[49] was used to confirm the unit cell dimensions and the crystal lattices. Solutions were obtained using direct methods which located the positions of the heavy atoms. Successive difference Fourier syntheses revealed all light atoms, which were assigned on the basis of their bond distances to the heavy atoms. The final refinement was obtained by introducing a weighting factor ($w = 1/[\sigma^2(F_o^2) + (0.0839)^2]$) and anisotropic thermal parameters for all non-hydrogen atoms in the $[OsO_3F][AsF_6]$ and $[OsO_3F][HF]_2[AsF_6]$ structures, giving a residual, R_1, of 0.0401 (wR_2 = 0.0797), 0.0325 (wR_2 = 0.0772), 0.0348 (wR_2 = 0.0864), 0.0558 (wR_2 = 0.1198), and 0.0858 (wR_2 = 0.1871) and maximum and minimum electron densities in the final difference Fourier map of 1.636/−1.397, 2.420/−1.763, 1.446/−1.280, 2.598/−2.327, and 2.209/−2.610 e $Å^{-3}$ for $[OsO_3F][AsF_6]$, $[OsO_3F][SbF_6]$, $[OsO_3F][HF]_2[AsF_6]$, $[OsO_3F][HF][SbF_6]$, and $[OsO_3F][Sb_3F_{16}]$, respectively. The residual electron densities were located around the heavy atoms. The crystal containing $[OsO_3F][SbF_6]$ was a twin; in addition to the diffraction spots for $[OsO_3F][SbF_6]$, diffraction spots were present that were indexed to give a cubic cell (a = 10.088(2) Å). The determination of the content of the cubic cell is still under investigation. As a consequence of the twinning, only the Os and Sb atoms could be refined anisotropically. The crystal of $[OsO_3F][HF][SbF_6]$ was a merohedral twin (ca. 40:60). Therefore, a proper absorption correction could not be performed and the fluorine and oxygen atoms were refined isotropically. In the structure of $[OsO_3F][Sb_3F_{16}]$, the Os atom was found on a special position ($\bar{4}$..) resulting in disorder among the three O and the F atoms of the cation. In addition, the fluorine atoms in the $Sb_3F_{16}^-$ anion were disordered between two orientations. As a consequence, the oxygen and fluorine atoms of the anion and cation could only be refined isotropically.

Raman Spectroscopy. The low-temperature Raman spectra of $[OsO_3F][AsF_6]$ (−150 °C), $[OsO_3F][HF]_2[AsF_6]$ (−140 °), $[OsO_3F][HF]_2[SbF_6]$ (−80 °C), and $[\mu\text{-}F(OsO_3F)_2][AsF_6]$ (−80 °C) were excited using the 647.1 nm line of a Kr ion laser (Lexel Laser, Inc., model 3550) and the spectra were recorded on a Jobin-Yvon Mole S-3000 triple spectrograph system as previously described.[41] The spectra were recorded in $^1/_4$-in. FEP sample tubes using the macrochamber of the instrument with a resolution of 1 cm^{-1} and a total of 10 reads each having 30 s integration times using laser powers of 100 mW. The low temperatures were achieved as previously described.[42]

The low-temperature Raman spectra of $[OsO_3F][Sb_3F_{16}]$ (−165 °C) and $[OsO_3F][HF][SbF_6]$ (−165 °C) were recorded on a Bruker RFS 100 FT Raman spectrometer using 1064-nm excitation as previously described.[4] The low-temperature spectra of $[OsO_3F][Sb_3F_{16}]$ and $[OsO_3F][HF][SbF_6]$ were recorded on powdered samples in a melting point capillary and in a $^1/_4$-in. FEP sample tube, respectively, using laser powers of 200 mW and a total of 1000 and 500 scans, respectively.

Nuclear Magnetic Resonance Spectroscopy. The ^{19}F NMR spectra (470.539 MHz) of $[OsO_3F][Sb_3F_{16}]$ in SbF_5 (SO_2ClF) solvent were recorded unlocked (field drift < 0.1 Hz h^{-1}) on a Bruker DRX-500 (11.7438 T) spectrometer using a 10-mm (5-mm) broad-band probe. The spectra of the SbF_5 (SO_2ClF) solutions were acquired in 64/16 (64) K memories with spectral width settings of 100/25 (50) kHz, yielding acquisition times of 0.328 (0.655) s and data point resolutions of 1.526 (0.763) Hz/data point; a pulse width of 2.5 μs was used. The ^{19}F NMR spectrum (282.409 MHz) of OsO_3F_2 with excess AsF_5 in HF solvent was recorded unlocked (field drift < 0.1 Hz h^{-1}) on a Bruker AC-300 (7.046 T) spectrometer using a 5-mm $^1H/^{13}C/^{19}F/^{31}P$ combination probe. The spectrum was acquired in a 64 K memory with a spectral width setting of 100 kHz, yielding an acquisition time of 0.328 s and data point resolution of 3.052 Hz/data point; a pulse width of 3 μs was used.

(47) *SMART and SAINT*, release 4.05; Siemens Energy and Automation Inc.: Madison, WI, 1996.
(48) Sheldrick, G. M. SADABS (Siemens Area Detector Absorption Corrections), personal communication, 1996.
(49) Sheldrick, G. M. *SHELXTL-Plus*, release 5.03; Siemens Analytical X-ray Instruments, Inc.: Madison, WI, 1994.

Calculations. The electron structure calculations were done at the DFT level.[50−54] The DFT geometry optimizations and frequency calculations were done with the program DGauss[55−58] on SGI computers. The calculations were carried out at the local level with the potential fit of Vosko, Wilk, and Nusair[59] for correlation and Slater exchange[60] and with the following basis sets: For H, O, F, Sb, and As, the DZVP polarized double-ζ basis set[61] was used (no polarization functions on H) with the A1 fitting set. For Os, the ECP and basis set of Hay and Wadt was used with the A1 fitting set derived for pseudopotentials within DGauss.[63,64] The geometries were optimized by using analytic gradient methods, and second derivatives were also calculated analytically. Atomic valencies following Mayer were calculated.[65−68] No scaling of the calculated vibrational frequencies was applied.

(50) Parr, R. G.; Yang, W. *Density-Functional Theory of Atoms and Molecules*; Oxford University Press: New York, 1989.
(51) Labanowski, J. K., Andzelm, J. W., Eds. *Density Functional Methods in Chemistry*; Springer-Verlag: New York, 1991.
(52) Ziegler, T. *Chem. Rev.* **1991**, *91*, 651.
(53) Salahub, D. R. In *Ab Initio Methods in Quantum Chemistry-II*; Lawley, K. P., Ed.; J. Wiley and Sons: New York, 1987; pp 447−520.
(54) Jones, R. O.; Gunnarsson, O. *Rev. Mod. Phys.* **1989**, *61*, 689.
(55) Andzelm, J.; Wimmer, E.; Salahub, D. R. In *The Challenge of d and f Electrons: Theory and Computation*; Salahub, D. R., Zerner, M. C., Eds.; ACS Symposium Series 394; American Chemical Society: Washington, DC, 1989; p 228.
(56) Andzelm, J. In *Density Functional Theory in Chemistry*; Labanowski, J., Andzelm, J., Eds.; Springer-Verlag: New York, 1991; p 155.
(57) Andzelm, J.; Wimmer, E. *J. Chem. Phys.* **1992**, *96*, 1280.
(58) DGauss is a density functional program which is part of Unichem and is available from Oxford Molecular.
(59) Vosko, S. H.; Wilk, L.; Nusair, M. *Can. J. Phys.* **1980**, *58*, 1200.
(60) Slater, J. C. *Phys. Rev.* **1951**, *81*, 385.
(61) Godbout, N.; Salahub, D. R.; Andzelm, J.; Wimmer, E. *Can. J. Chem.* **1992**, *70*, 560.
(62) Hay, P. J.; Wadt, W. R. *J. Chem. Phys.* **1985**, *82*, 299.
(63) Chen, H.; Krasowski, M.; Fitzgerald, G. *J. Chem. Phys.* **1993**, *98*, 8710.
(64) Lee, C.; Chen, H. Unpublished results. See: UniChem Manual Version 3.0−5.0.
(65) Mayer, I. *Chem. Phys. Lett.* **1983**, *97*, 270.
(66) Mayer, I. *Theor. Chim. Acta* **1985**, *67*, 315.

Acknowledgment. We thank the donors of the Petroleum Research Fund, administered by the American Chemical Society, for support of this work under Grant ACS-PRF No. 28284-AC3. This research was performed, in part, using the Molecular Science Computing Facility (MSCF) in the William R. Wiley Environmental Molecular Sciences Laboratory at the Pacific Northwest National Laboratory. The MSCF is funded by the Office of Biological and Environmental Research in the U.S. Department of Energy. The Pacific Northwest Laboratory is operated by Battelle for the U.S. Department of Energy under Contract DE-AC06-76RLO 1830. We also thank the Ontario Ministry of Education and the Richard Fuller and James A. Morrison Memorial Funds for the award of graduate scholarships to M.G. and the Canada Council for the award of a Killam Research Fellowship (1998 and 1999) to G.J.S. We also thank Dr. William J. Casteel for his help with some of the exploratory experiments and Dr. Hélène P. A. Mercier for her help with the solution of the crystal structure of $[OsO_3F][SbF_6]$.

Supporting Information Available: Unit cell diagrams for $[OsO_3F][AsF_6]$ (Figure S9), $[OsO_3F][HF]_2[AsF_6]$ (Figure S10), $[OsO_3F][HF][SbF_6]$ (Figure S11), and $[OsO_3F][Sb_3F_{16}]$ (Figure S12), X-ray crystallographic files, in CIF format, for the structure determinations of $[OsO_3F][AsF_6]$, $[OsO_3F][SbF_6]$, $[OsO_3F][HF]_2[AsF_6]$, $[OsO_3F][HF][SbF_6]$, and $[OsO_3F][Sb_3F_{16}]$, calculated dihedral angles for $(FO_3Os\text{--}(HF)_2\text{--}FPnF_5)_2$ (Pn = As, Sb) (Table S11), and Mulliken charges and Mayer valencies for $(FO_3Os\text{--}FPnF_5)_2$ and $(FO_3Os\text{--}(HF)_2\text{--}FPnF_5)_2$ (Table S12). This material is available free of charge via the Internet at http://pubs.acs.org.

IC0107680

(67) Mayer, I. *Int. J. Quantum Chem.* **1986**, *29*, 73.
(68) Mayer, I. *Int. J. Quantum Chem.* **1986**, *29*, 477.